LITHOS 436–437 (2023) 106973

Contents lists available at ScienceDirect

LITHOS

journal homepage: www.elsevier.com/locate/lithos

Fluid flow in the subduction channel: Tremolite veins and associated blackwalls in antigoritite (Villa Clara serpentinite mélange, Cuba)

Lidia Butjosa [a], Aitor Cambeses [b,*], Joaquín A. Proenza [a], Idael F. Blanco-Quintero [c], Samuele Agostini [d], Manuel Antonio Iturralde-Vinent [e], Antonio Garcia-Casco [b,f]

[a] Departament de Mineralogia, Petrologia i Geologia Aplicada, Universitat de Barcelona, 08028 Barcelona, Spain
[b] Departamento de Mineralogía y Petrología, Universidad de Granada, 18071 Granada, Spain.
[c] Departamento de Ciencias de la Tierra y del Medio Ambiente, Universidad de Alicante, 03080 Alicante, Spain
[d] Istituto di Geoscienze e Georisorse, CNR, 56124 Pisa, Italy
[e] Academia de Ciencias de Cuba, La Habana, Cuba
[f] Instituto Andaluz de Ciencias de la Tierra (CSIC-UGR), 18100, Armilla, Granada, Spain

ARTICLE INFO

Keywords:
Antigoritite
Abyssal peridotite
Subduction
Fluid infiltration
Metasomatism
Mélange
Cuba
Caribbean

ABSTRACT

Exotic blocks of massive antigorite-serpentinite (antigoritite) document a deep-seated subduction channel in the Villa Clara serpentinite-matrix mélange, central Cuba. The petrological and geochemical characteristics of antigoritite allow distinguishing two types of rock: i) antigoritite and ii) dolomite-bearing antigoritite. Both types are intimately related in field exposures and represent deep peridotite infiltrated by H_2O-CO_2 fluid mixtures that triggered antigoritization and local carbonation. Fluid infiltration continued after antigoritization forming a vein network as a potential response to hydrofracturing that precipitated tremolitite in the veins and triggered fluid-antigoritite reaction forming blackwalls. The mineralogical and chemical zoning in the blackwalls (Atg + Chl + Tr adjacent to antigoritite and Chl + Tr adjacent to the tremolitite vein) attest for multi-step metasomatic processes during fluid-rock interaction characterized by advection of infiltrating fluid towards the blackwall and, possibly, by diffusion out of the blackwall towards the fluid-filled vein. Tentative thermodynamic modeling of the blackwall domain Atg + Chl + Tr points vein network formation at 400–500 °C and 5–10 kbar during exhumation in the subduction channel, suggesting the infiltration of deep-seated pressurized fluid that triggered hydrofracturing. The chemical compositions of antigoritites, veins and blackwalls indicate a LILE- and LREE-enriched fluid evolved from the subducting plate, while Sr—Nd isotope systematics are compatible with an external fluid composed of a mixture of fluids evolved from sediments and, probably to a lesser extent, altered oceanic crust.

1. Introduction

Exhumed subduction channel mélanges are natural laboratories for the study of fluid-rock interaction and mass- transfer at the subduction interface and the subduction channel. Fluid evolved from subducting slabs is able to flow and transport elements over large distances in the subduction environment, triggering chemical-mechanical processes that are responsible for hydrofracturing, seismicity and varied metasomatic transformations and mass recycling in the subduction-suprasubduction system (Ague, 2017; Angiboust et al., 2014, 2017, 2021a, 2021b; Bebout, 1991, 2007, 2014; Bebout and Penniston-Dorland, 2016; Beinlich et al., 2010; Blanco-Quintero et al., 2011c; Bouilhol et al., 2012; Cannaò et al., 2015, 2016, 2020; Connolly and Galvez, 2018; Gilio et al., 2019; Hermann et al., 2006; Konrad-Schmolke et al., 2011; Lázaro et al., 2011; Muñoz-Montecinos et al., 2020, 2021a, 2021b; Penniston-Dorland et al., 2012; Scambelluri et al., 2004, 2019; Scambelluri and Tonarini, 2012; Sorensen et al., 2010; Spandler et al., 2011; Taetz et al., 2016; Vitale-Brovarone et al., 2014; Zack and John, 2007).

Tracking fluid flow and determining potential fluid sources is possible after inspection of appropriate subducted lithologies. In general terms, the fluid cycle in the subduction environment shallower than sub-arc depths can be characterized as follows. At oceanic fault zones and

* Corresponding author.
E-mail addresses: lbutjosa@ub.edu (L. Butjosa), aitorc@ugr.es (A. Cambeses), japroenza@ub.edu (J.A. Proenza), if.blanco@ua.es (I.F. Blanco-Quintero), s.agostini@igg.cnr.it (S. Agostini).

https://doi.org/10.1016/j.lithos.2022.106973
Received 30 June 2022; Received in revised form 26 October 2022; Accepted 24 November 2022
Available online 1 December 2022

core-complexes, and at trenches during bending and related faulting of the downgoing oceanic plate, seawater is introduced in the oceanic lithosphere, promoting partial to total hydration of basalt, gabbro and peridotite (Ague and Nicolescu, 2014; Boschi et al., 2008; Breeding et al., 2004; Delacour et al., 2008; Deschamps et al., 2011; Hart et al., 1999; Humphris and Thompson, 1978; Kodolányi et al., 2012; Padrón-Navarta et al., 2010; Ranero et al., 2003; Snow et al., 1994). Upon subduction, these hydrated rock units are transformed into blueschist, eclogite and antigoritite and higher-grade hydrated ultramafic granofels such as chlorite metaharzburgite (Hacker, 2008). Devolatilization triggered during prograde subduction-related metamorphism of these rocks and associated metasediments produces fluids of variable composition depending on source lithology and thermal regime (Alt et al., 2013; Bebout, 1991; Hacker, 2008; Marchesi et al., 2013; Molina and Poli, 2000; Padrón-Navarta et al., 2011; Piccoli et al., 2016; Scambelluri et al., 2019; Schmidt and Poli, 2014; Spandler and Pirard, 2013; Van Keken et al., 2011). The evolved fluids infiltrate subducted and upper-plate material following diffuse and channelized flow (the latter due to eventual mechanical failure including hydrofracturing) that allow mixing of variably sourced fluids and trigger fluid-rock interactions and metasomatism (Angiboust et al., 2014, 2021a, 2021b; Muñoz-Montecinos et al., 2020, 2021a, 2021b; Padrón-Navarta et al., 2010; Piccoli et al., 2021; Soret et al., 2016).

Evidence of fluid/rock interaction at the subduction factory has been documented by means of detailed mineralogical-geochemical studies of high-pressure rocks of igneous and sedimentary origin and eventual metasomatic rinds around them, in many cases forming part of high-pressure mélanges that represent fragments of the subduction channel (Bebout and Penniston-Dorland, 2016; Cárdenas-Párraga et al., 2021; Harlow and Sorensen, 2005; Penniston-Dorland et al., 2010, 2012, 2014; Sorensen et al., 1997; Sorensen and Grossman, 1989; Ukar and Cloos, 2013), and in veins emplaced in high pressure rocks (Cárdenas-Párraga et al., 2017; John et al., 2008; Muñoz-Montecinos et al., 2020, 2021b; Plümper et al., 2017; Scott et al., 2019; Spandler et al., 2011; Taetz et al., 2016; Tarling et al., 2019; van der Straaten et al., 2008; Zack and John, 2007). These studies suggest fluids enriched in fluid-mobile Large Ion Lithophile Elements (LILE: K, Ba, Rb, Cs), indicating a sedimentary and/or altered oceanic crust source. However, determining the relative contribution of slab sources in the infiltrating fluid is only possible after detailed inspection of the elemental and isotopic compositions of subducted lithologies (Cannaò et al., 2016; Debret et al., 2013; Deschamps et al., 2010; King et al., 2006; Lafay et al., 2013; Penniston-Dorland et al., 2012; Scambelluri et al., 2001, 2004, 2019).

In this work, we use mineral and whole rock major and trace element and isotopic compositions of high-presssure antigoritite blocks, veins within them and associated blackwalls to characterize fluid-rock interactions in the subduction environment. Tremolite-veins rimmed by metasomatic blackwalls hosted in tectonic blocks of antigoritite from the VCSM, central Cuba, document fluid infiltration, likely triggered by hydrofracturing, and fluid-driven mass transfer at depth. We offer an integrated petrological, geochemical and isotopic study in an effort to constraining the intervening processes and reservoir sources of fluids in the subduction environment.

2. Geological background

The Proto-Caribbean basin (related to the Central Atlantic) formed in between the Americas during Jurassic-late Cretaceous time and started westerly-directed subduction below the Pacific (Farallon plate) in the early Cretaceous, forming backarc, forearc and arc settings in the leading edge of the Caribbean plate (Boschman et al., 2014; Escuder-Viruete et al., 2011a, 2014; Hu et al., 2022; Lázaro et al., 2016; Lidiak and Anderson, 2015; Pindell et al., 2012; Pindell and Kennan, 2009; Rojas-Agramonte et al., 2011; Rui et al., 2022). High pressure complexes formed in the associated subduction zone, including serpentinite-matrix mélanges bearing tectonic blocks of mostly oceanic- and volcanic arc-derived blueschist and eclogite facies rocks (Blanco-Quintero et al., 2010, 2011a, 2011b; Escuder-Viruete et al., 2011a; Escuder-Viruete and Castillo-Carrión, 2016; Garcia-Casco et al., 2002, 2006, 2008b; Lázaro et al., 2009; Lázaro and Garcia-Casco, 2008; Somin and Millán, 1981) and coherent subducted passive margin sequences/terranes (Cruz-Gámez et al., 2016; Despaigne-Diaz et al., 2016, 2017; Escuder-Viruete et al., 2011b; Escuder-Viruete and Pérez-Estaún, 2013; Garcia-Casco et al., 2008a). Convergence largely consumed the Proto-Caribbean by latest Cretaceous-early Tertiary time, triggering collision of the Caribbean arc system with the North American margin, the tectonic emplacement of ophiolitic and volcanic arc units and subducted oceanic and passive margin terranes onto the margin and the formation of the Caribbean Cretaceous-Tertiary orogenic belt (Cruz-Orosa et al., 2012; Escuder-Viruete et al., 2016; Garcia-Casco et al., 2008a; Iturralde-Vinent et al., 2008; Saura et al., 2008; van Hinsbergen et al., 2009). Remains of these units are well exposed in Cuba (Fig. 1).

Cuba is composed of imbricated passive margin, ophiolitic, volcanic arc and high-pressure units that run parallel to the island along >1000 km (Iturralde-Vinent, 1996; Iturralde-Vinent et al., 2016; Lewis et al., 2006). Most ages of ophiolitic and volcanic arc rocks comprise the period of 135–70 Ma (Hall et al., 2004; Hu et al., 2022; Iturralde-Vinent et al., 1996; Lázaro et al., 2016; Llanes Castro et al., 2018; Proenza et al., 2006; Rojas-Agramonte et al., 2010, 2011, 2016; Rui et al., 2022), similar to the age range of high-pressure rocks, 125–60 Ma (Blanco-Quintero et al., 2011d; Despaigne-Diaz et al., 2016, 2017; Hu et al., 2022; Iturralde-Vinent et al., 1996; Lázaro et al., 2009; Schneider, 2000; Schneider et al., 2004; Stanek et al., 2006, 2019).

The Villa Clara serpentinitic mélange (VCSM) in central Cuba tectonically lies, respectively, above and below the Bahamian borderland units related to the North American passive margin and the Cretaceous volcanic arc sequences (Fig. 1B and C). The latter include ca. 135–70 Ma tholeiitic to calc-alkaline rocks intruded by arc-related granitoids that also intrude the VCSM (Díaz de Villalvilla, 1997; Díaz de Villalvilla et al., 2003; Rojas-Agramonte et al., 2010, 2011). The VCSM is composed of a wide range of m- to km-sized bodies of ophiolitic, volcanic arc and passive margin materials and high-pressure tectonic blocks of metabasite (eclogite and blueschist), metaultramafic (antigoritite, chloritite, tremolitite-actinolitite) and metasedimentary composition embedded in a low-pressure serpentinized ultramafic matrix (Álvarez-Sánchez et al., 1991; Álvarez-Sánchez and Bernal-Rodríguez, 2015; Butjosa et al., 2022; Ducloz and Vuagnat, 1962; Garcia-Casco et al., 2002, 2006; Kanchev et al., 1978; Somin and Millán, 1981). The low-pressure ophiolitic rocks of basaltic composition are of forearc and island arc tholeiitic signature (Butjosa et al., 2022; Kerr et al., 1999).

Two types of serpentinites have been identified based on textural and mineralogical characteristics: 1) low-T lizardite-serpentinite with relics of mantle minerals and pseudomorphic texture that constitutes the serpentinitic matrix of the VCSM, and 2) ultramafic blocks of high-T antigorite-serpentinite (antigoritite) with no relics of mantle minerals and non-pseudomorphic interlocking texture that locally wrap around high pressure blocks of eclogite and hence form part of the suite of exotic high-P blocks present in the mélange (Auzende et al., 2002; Butjosa et al., 2022; Hattori and Guillot, 2007; Somin and Millán, 1981). The geochemical compositions of the low-T serpentinized peridotites indicate the presence of both abyssal and forearc peridotites while antigoritites share characteristics of subducted abyssal peridotite (Butjosa et al., 2022; Deschamps et al., 2011, 2012; Hattori and Guillot, 2007). A dated eclogite block metamorphosed to *c.* 20 kbar and 570–600 °C has yielded amphibole- and phengite-Ar/Ar- and phengite-omphacite-whole rock Rb/Sr isochron ages ranging from 103 to 123 Ma (Garcia-Casco et al., 2002, 2006; Schneider, 2000). Most K—Ar ages of eclogite and amphibolitized eclogite blocks in the Villa Clara serpentinitic mélange and other serpentinite-matrix mélanges of west-central Cuba cluster at *c.* 110 Ma (Iturralde-Vinent et al., 1996). Paleocene-Eocene *syn*-tectonic sedimentary formations, on the other hand, indicate that the obduction of the serpentinitic mélange onto the passive margin sequences occurred

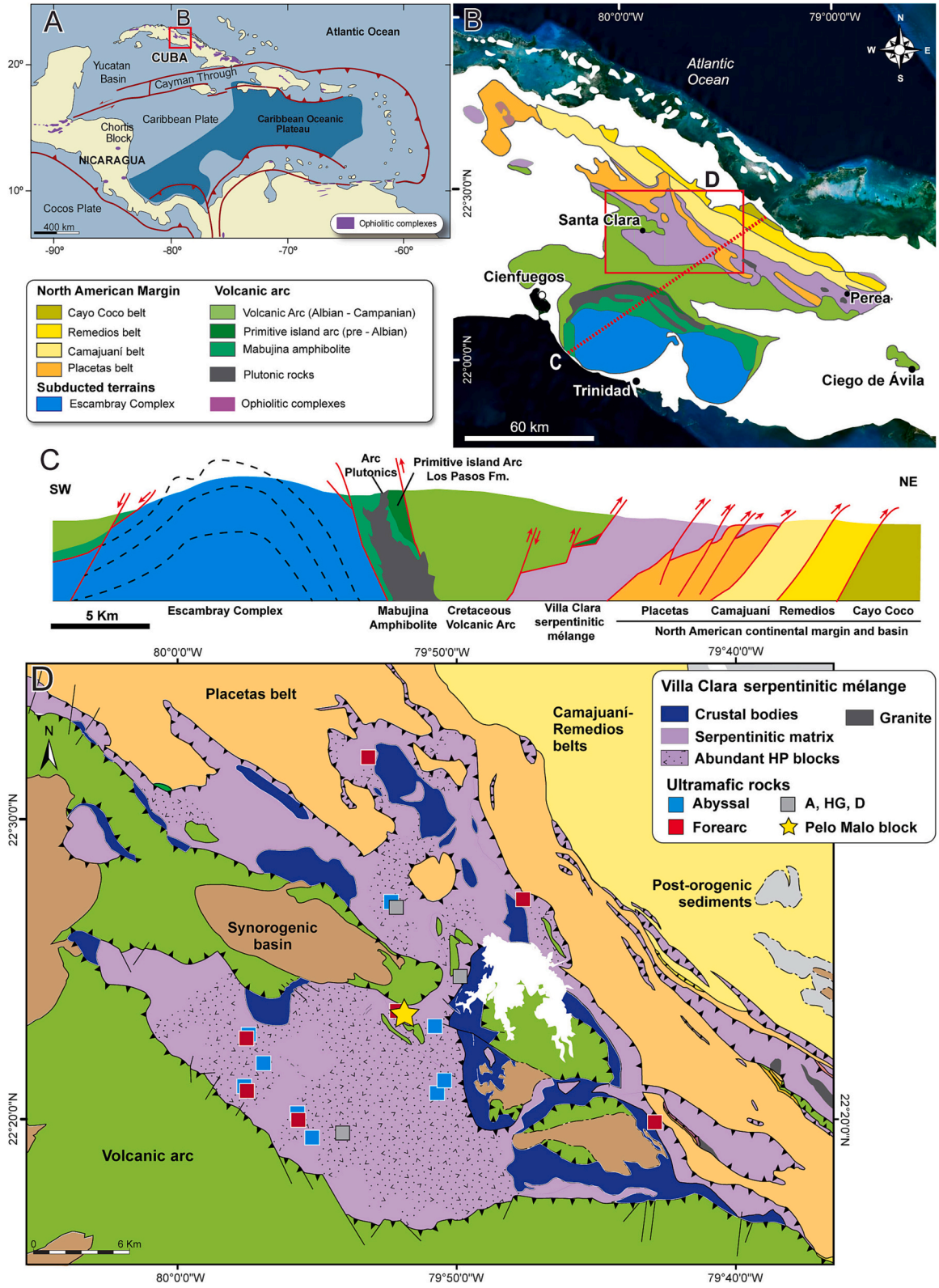

Fig. 1. A) Plate tectonic configuration of the Caribbean region, including ophiolitic complexes. B) - C) Geological map and cross-section of central Cuba showing the basic geologic features (Iturralde-Vinent, 1998). D) Geological map of the Villa Clara region (red rectangle in B) with the main geologic features (Álvarez-Sánchez et al., 1991; García Delgado et al., 1998; Kanchev et al., 1978) and location of studied samples. Also shown are the locations of samples of low-T lizardite-bearing serpentinites with abyssal and forearc geochemical signatures (Butjosa et al., 2022) and of samples studied by Auzende et al. (2002), Deschamps et al. (2012) and Hattori and Guillot (2007) (gray squares labeled A, HG, D). (For interpretation of the references to colour in this figure legend, the reader is referred to the web version of this article.)

shortly after *c*. 70 Ma and continued during the Paleocene-Eocene in a context of sequential terrane (Caribeana) subduction/accretion and arc-continental margin collision. All these geological, mineralogical, petrological, geochemical and geochronological data indicate formation of a deep-seated antigoritite-matrix mélange in the Caribbean subduction channel by ca. 125 Ma rapidly followed by synsubduction exhumation to shallow depth along the subduction channel during 100–110 Ma, when the high-P material was retrogressed and mixed with low-pressure ophiolitic forearc serpentinized mantle until obduction triggered a second mélange-forming event (Butjosa et al., 2022; Garcia-

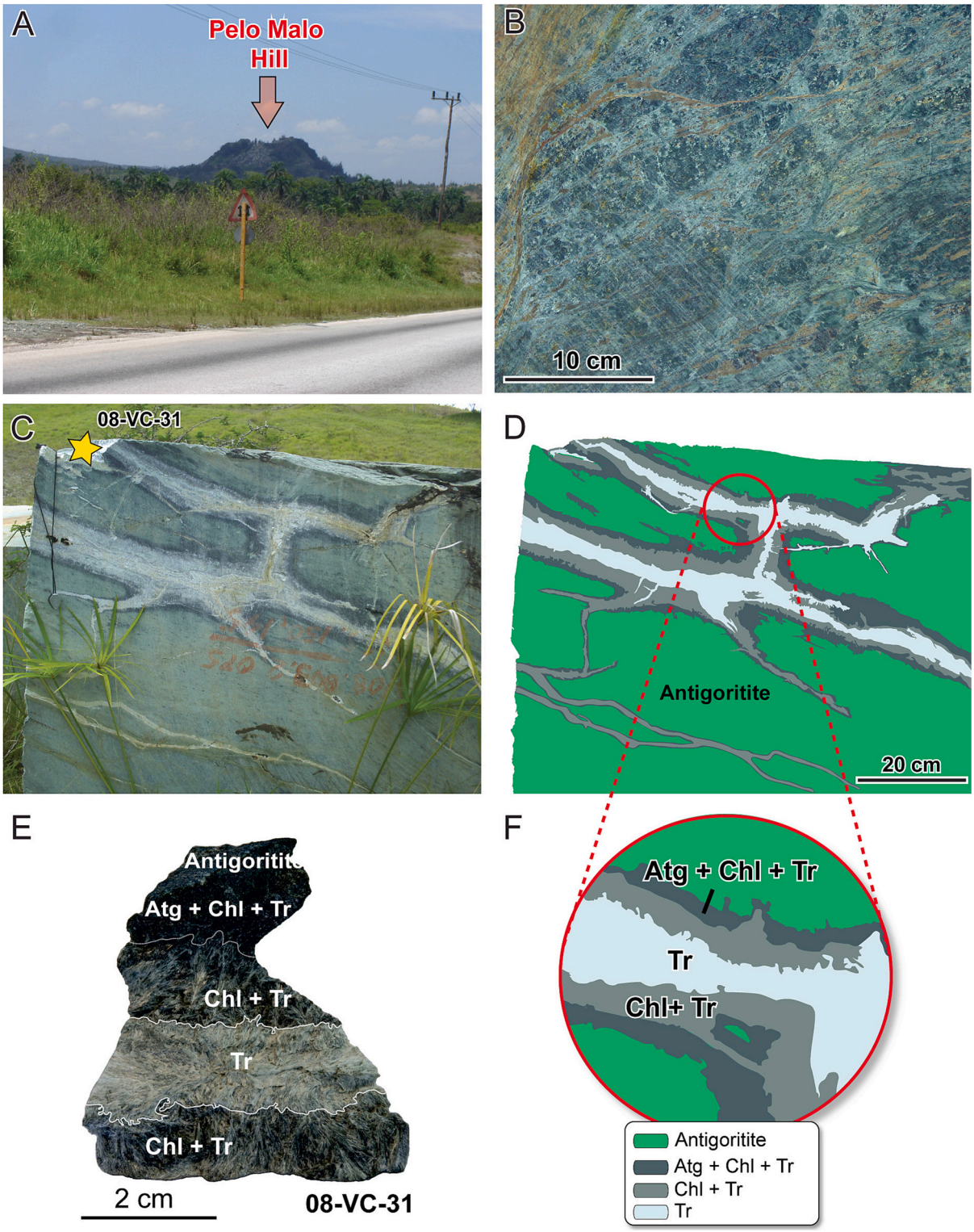

Fig. 2. A) Field view of the Pelo Malo antigoritite megablock in the flat landscape made of lizardite-bearing serpentinized peridotites (Butjosa et al., 2022). B) Pelo Malo antigoritite showing foliation and brownish regions richer in dolomite. C) and D) Detail of veined hydrofracturing brittle structure within antigoritite; sample 08-VC-31 was taken from the location of the star. E) Hand-specimen of the vein and metasomatic domains. F) Zoom inside the vein structure showing Atg + Chl + Tr and Chl + Tr domains and tremolite vein.

Casco et al., 2002, 2006, 2008a).

It has been proposed that the VCSM mélange is in fact made of two mélanges, the low pressure Descanso ophiolitic mélange tectonically on top of the high pressure Santa Clara mélange (Álvarez-Sánchez et al., 1991; Álvarez-Sánchez and Bernal-Rodríguez, 2015). However, our observations (see also Kanchev et al., 1978) have recognized high-pressure blocks in both mélanges as mapped by Álvarez-Sánchez et al. (1991) and it is not uncommon to see the presence of high-pressure blocks adjacent to (a few meters apart from) low-P/unmetamorphosed blocks. Furthermore, the geochemical diversity of ultramafic rocks do not correlate with the mapped areas of both mélanges (Butjosa et al., 2022). Hence, we agree with these authors in that VCSM is a composite mélange (polygenic polyphasic mélange, in their words) but it will be treated here as a single but complex geologic complex made of low-T serpentinized peridotite enclosing not-subducted oceanic, volcanic arc and passive margin-derived bodies and fragments/blocks of a high-P mélange (antigoritite+HP blocks) (Fig. 1D).

3. Field relations

High-T antigoritite is particularly well exposed in the Pelo Malo megablock, to the east of Santa Clara city (Figs. 1D and 2A). The surface area of the megablock is 55,150 m^2 and consists of bluish to greenish massive to strongly sheared antigoritite (Fig. 2B and C) enclosed within low-T lizardite-serpentinite of forearc geochemical signature (Fig. 1D; Butjosa et al., 2022). The type of rock and field relations are similar to those of smaller antigoritite blocks. However, the Pelo Malo antigoritite shows unusual tremolite vein networks and associated zoned blackwalls at the vein-rock contact (Fig. 2C to 2F) that document a process of fluid infiltration at depth likely triggered by hydrofracturing (e.g., Muñoz-Montecinos et al., 2020, 2021b). The vein-wall rock structure is formed by four domains: i) antigoritite host rock, ii) antigorite + chlorite + tremolite (Atg + Chl + Tr) blackwall outer band, iii) chlorite + tremolite (Chl + Tr) blackwall inner band and iv) tremolite vein (Tr-vein) (Fig. 2E and F). This vein structure has not been identified in nearby lizardite serpentinites, reinforcing the view of an exotic character of the Pelo Malo megablock.

4. Analytical methods

Fresh samples of antigoritite (6 samples), metasomatic blackwall domains and vein (3 samples) were analyzed for detailed geochemical study after careful mechanical fragmentation of the different domains. The samples were crushed and powdered with an agate mortar and mill. Table 1S shows whole-rock major and trace elements composition of the studied samples. Major elements and Zr were analyzed with a Philips Magix Pro (PW-2440) X ray fluorescence (XRF) equipment at the University of Granada (Centro de Instrumentación Científica, CIC-UGR) after fusion with lithium tetraborate; typical precision of XRF analyses was better than ±1.5% for an analyte concentration of 10 wt% and ± 4% for concentrations of <10 wt% (major oxides) and ± 0.2% for 5 ppm Zr. Trace element concentrations were determined using a quadrupole NEXION 300d Inductively Coupled Mass Spectrometry (ICP-MS) at CIC-UGR after HNO_3 + HF digestion of 0.1 g of sample powder in a Teflon-lined vessel at 180 °C and 200 psi for 30 min, evaporation to dryness, and subsequent dissolution in 100 ml of 4 vol% HNO_3; the precision was better than ±5% for analyte concentrations of 10 ppm.

Nd and Sr isotopic data were obtained in blackwall domain Chl + Tr and Tr-vein, while only Sr data are reliable in antigoritite (Table 2S). Samples for Sr and Nd isotope analysis were digested with HNO_3 + HF using ultra-clean reagents and analyzed by Thermal Ionization Mass Spectrometry (TIMS) in a Finnigan Mat 262 spectrometer after chromatographic separation with ion-exchange resins at CIC-UGR. Normalization values were $^{86}Sr/^{88}Sr = 0.1194$ and $^{146}Nd/^{144}Nd = 0.7219$. Blanks were 0.6 and 0.09 ng for Sr and Nd respectively. The external precision (2σ), estimated by analyzing 10 replicates of the standard WS–E (Govindaraju, 1994) was better than ±0.003% for $^{87}Sr/^{86}Sr$ and ± 0.0015% for $^{143}Nd/^{144}Nd$. $^{87}Sr/^{86}Rb$ and $^{147}Sm/^{144}Nd$ were directly determined by ICP-MS following the method developed by Montero and Bea (1998), with a precision better than ±1.2% and ± 0.9% (2σ), respectively.

Micro-Raman spectra of serpentine group minerals in antigoritite samples were acquired at the Centres Científics i Tecnològics of Barcelona University (CCIT-UB), using a dispersive spectrometer Jobin Yvon LabRam-HR800 equipped with an Olympus BXFM optical microscope (using a 100× objective lens) and 600 mm focal length spectrograph equipped with a CCD 5 mW laser power working at 785 nm. In order to optimize the signal-to-noise ratio the laser beam size was set to 10 μm. Spectra were acquired using 8 scans of 30 s per spectral region, and processed using NGS-Labspec (version. 5.33.14) software. An automatic baseline subtraction was performed and serpentine phases were identified by the spectral characteristics (Groppo et al., 2006).

Mineral and end-member abbreviations are after Whitney and Evans (2010). Mineral compositions antigoritite, Atg + Chl + Tr and Chl + Tr blackwall domains and the Tr-vein have been acquired with a JEOL JXA-8230 microprobe at CCIT-UB and a CAMECA SX–100 at CICU-GR (20 keV accelerating potential, 20 nA beam current). Analyses are given in Table 3S. Fe^{3+} in amphibole was calculated after normalization to 23 oxygens following Hawthorne et al. (2012). Magnetite and ferrian chromite were normalized to 3 cations and 4 oxygens per formula unit (pfu) with Fe^{3+} estimated by stoichiometry. Chlorite, antigorite and dolomite were normalized to 28, 14 and 6 oxygens, respectively, considering Fe total as Fe^{2+}. Elemental X-ray (WDS) and back-scattered electron (BSE) images were obtained with the CAMECA SX–100 machine operated at 20 keV and 300 nA, a focused beam, step (pixel) size of 14 μm and counting time of 30 ms/pixel. The images were processed with DWImager software (Garcia-Casco, 2007). The X-ray signals were quantified using internal standards (EMP point analyses) in the imaged region and the ZAF correction procedure of Bence and Albee (1968; see Garcia-Casco, 2007 for details). The quantified XR maps (colour-coded; expressed in wt%) were clipped to mask out holes, polish defects and all other mineral phases, and the masked images were overlain onto the corresponding BSE image that contains the textural information of the imaged areas.

Mineral assemblages in the CNFMASH system were plotted in the tetrahedral MASH diagram in Fig. 9 using software CSpace (Torres-Roldan et al., 2000) after projection from tremolite and appropriate exchange vectors (as indicated in the figure) using the Singular Value Decomposition method (Fisher, 1989, 1993). For restoring the anhydrous mantle mineralogy of the samples in Fig. 5A, the bulk composition of studied samples were transformed to mineral components olivine, orthopyroxene, clinopyroxene and spinel. The composition space considered here is 8-dimensional, as defined by the chemical components SiO_2-Al_2O_3-Cr_2O_3-FeO-MnO-MgO-NiO-CaO (TiO_2, Na_2O, K_2O and P_2O_5 are neglected due to their low amounts in the samples considered; note, also, that because independent Fe_2O_3 and FeO estimates are not known, they are not considered as independent components and total iron is expressed as FeO; finally, because we are interested in the anhydrous mantle mineralogy, H_2O is neglected). The definition of the new set of 8 chemical species involves minerals and exchange vectors (mathematical operators that allow condensation of the composition space), convenient for visualization of the whole 8-dimensional chemical system in the Ol-Opx-Cpx diagram of Le Maitre et al. (2005) (Fig. 5A) after projection from spinel and exchange vectors. The minerals are calculated in oxy-equivalent (gram-oxygen) units since this measure of component abundance has the advantage of being an estimate of the volume of solids in which oxygen is the only major anion (Brady and Stout, 1980; Thompson, 1982). The calculations and projections were performed using software CSpace (Torres-Roldan et al., 2000). A full description of the method and applications is presented by Garcia-Casco et al. (2020).

The P-T phase diagram (pseudosection) of Atg-Chl-Tr blackwall

domain was calculated in the CaO-FeO-MgO-Al_2O_3-SiO_2-H_2O system using PERPLE_X software (Connolly, 1990, version 6.6.8). The standard state thermodynamic data are from Holland and Powell (2011) and the following solid solution models were used: antigorite (Padrón-Navarta et al., 2013), orthopyroxene and clinopyroxene (Holland and Powell, 1996), olivine, chlorite, talc, tremolite and anthophyllite (Holland et al., 1998). The major element composition of the Atg + Chl + Tr domain used for pseudosection calculation was calculated by means of the quantified XR-maps using 2,308,565 pixels (i.e., calculated analyses), which yielded SiO_2 = 41 wt% ± 0.01, Al_2O_3 = 9.31 wt% ± 0.02, FeO =

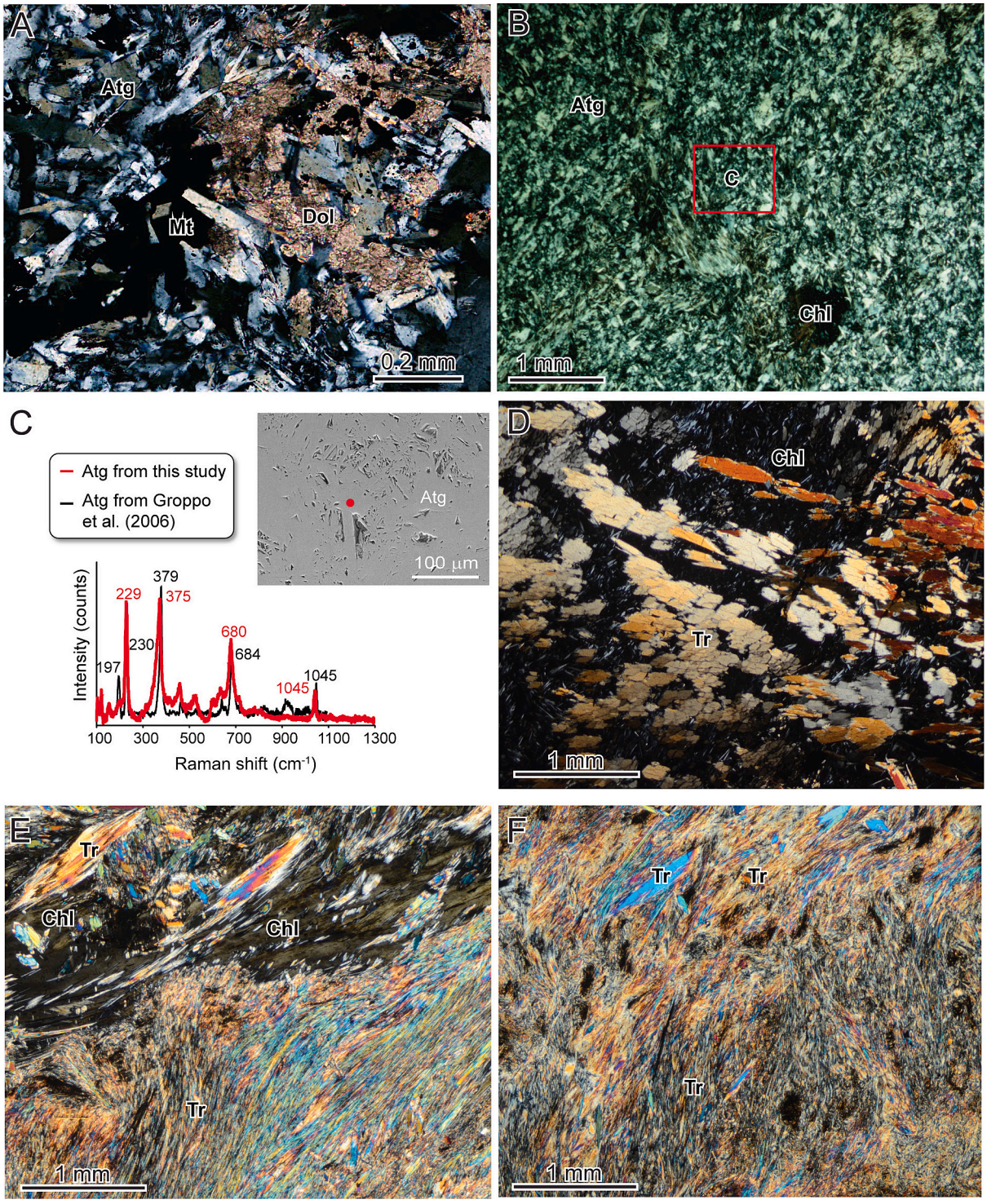

Fig. 3. Plane-polarized light (crossed polars) photomicrographs and BSE image of antigoritite and vein domains. A) Dolomite-bearing antigoritite showing antigorite-dolomite intergrowths. B) Antigoritite showing interpenetrating texture and chlorite blasts. C) BSE image of the area indicated in B showing blades of antigorite and Raman spectrum (red dot) (Groppo et al., 2006 for comparison). D) Chlorite + tremolite domain with abundant euhedral crystals of tremolite in a matrix of chlorite. E) Sharp contact between chlorite + tremolite domain and tremolite vein; note intense deformation. F) Tremolite vein showing deformed fibrous crystals with variable orientation and local euhedral crystals of greater size. (For interpretation of the references to colour in this figure legend, the reader is referred to the web version of this article.)

5.49 wt% ± 0.01, MgO = 29.13 wt% ± 0.01 and CaO = 4.13 wt% ± 0.02 (error 2σ calculated at 95% of confidence interval), and assuming H_2O saturation.

5. Mineral assemblages and textural relations

Antigoritite has a massive structure and strongly foliated and brecciated fabric denoting significant strain during and after serpentinization. Antigoritite bears minor chlorite+ferrian chromite+magnetite as transformation products of former chromian spinel, with occasional ilmenite and Fe—Ni sulfide and dolomite locally joining this assemblage (Fig. 3A and B). As opposed to low-T lizardite-bearing serpentinized peridotites of the VCSM (Butjosa et al., 2022), relicts of mantle phases (olivine, pyroxenes and spinel) and pseudomorphic textures are completely absent in antigoritite, and neither lizardite nor chrysotile were found in Raman spectra (Fig. 3C). Instead, antigorite develops non-pseudomorphic interpenetrating texture with blades of variable size, from 1 mm to 20 μm in length (Fig. 3B and C). When present, dolomite appears intergrown with antigorite (Fig. 3A), indicating infiltration of a CO_2-H_2O fluid during antigoritization. This process likely occurred along relatively diffuse network of fractures/veins/foliation during deformation (Fig. 2B).

The outer Atg + Chl + Tr blackwall domain is characterized by unoriented blades of antigorite (0.1 to 0.5 mm in length) intergrown with chlorite and dispersed euhedral crystals of tremolite that are 0.5 to 1 mm in length (Fig. 4). Towards the inner Chl + Tr domain the abundance of antigorite decreases, where it appears as small blades of 0.05–0.2 mm (Fig. 4), while tremolite abundance increases. The interface between the Chl + Tr blackwall domain and the Tr-vein is sharp, denoting that the latter corresponds to the locus of direct crystallization from fluid in an open fracture (Figs. 2, 3E, F and 4). The Tr-vein has dispersed euhedral shaped tremolite (c. 0.5–0.8 mm) within fibrous aggregates arranged in areas of variable orientation. Common textures include fan-shaped tremolite clusters (1 mm to up to 1 cm in length; Fig. 3E and F). Changes in orientation of fibers and oriented deformation fabrics in the vein and the adjacent Chl + Tr domain indicate that the vein concentrated shear deformation during and after fluid infiltration and crystallization. Dispersed chlorite-rich clusters within the vein are interpreted as mechanically detached fragments of the Chl + Tr domain (Fig. 4). Dolomite or other carbonates have not been detected in the blackwall domains and vein, indicating compositional differences in the fluids involved in the veining and antigoritization stages and, hence, that veining formation ensued antigoritization, as indicated by replacement of antigoritite in the blackwall (Fig. 4).

6. Mineral composition

Antigorite from antigoritite has Mg = 5.37–5.58 and Al = 0.08–0.25 pfu and Mg# [= Mg/(Mg + Fe^{2+})] = 0.96–0.97. The Al content of antigorite increases while Fe, Mg and Si decrease towards the blackwall (Fig. 4), denoting the tschermak exchange vector (Si(Mg, Fe)-Al_{-2}) (Fig. 4, Figs. 1S and 2S, Table 3S). In the Atg + Chl + Tr domain, antigorite has Mg = 4.93–5.26 and Al = 0.04–0.44 pfu. In this domain and in relicts within the Chl + Tr domain, antigorite shows negative Fe—Mg correlation, with higher Fe and lower Mg# (0.90–0.92) towards the vein, indicating the $FeMg_{-1}$ exchange (Fig. 2S). The distribution of Cr is irregular and related to the replacement of chromian spinel (top-right of the Cr image, Fig. 4A).

Chlorite in antigoritite, blackwall domains and vein has Si, Mg and Mg# ranging 6.32–6.64 pfu, 8.83–9.44 pfu and 0.90–0.91, respectively (Fig. 2S; Table 3S), typical of clinochlore. Chlorite in antigoritite surrounds magnetite and has the highest Cr contents (0.27–0.84 pfu), as expected for replacements after chromian spinel (Fig. 4B). Two contrasted chemical compositions are observed based on textural position in

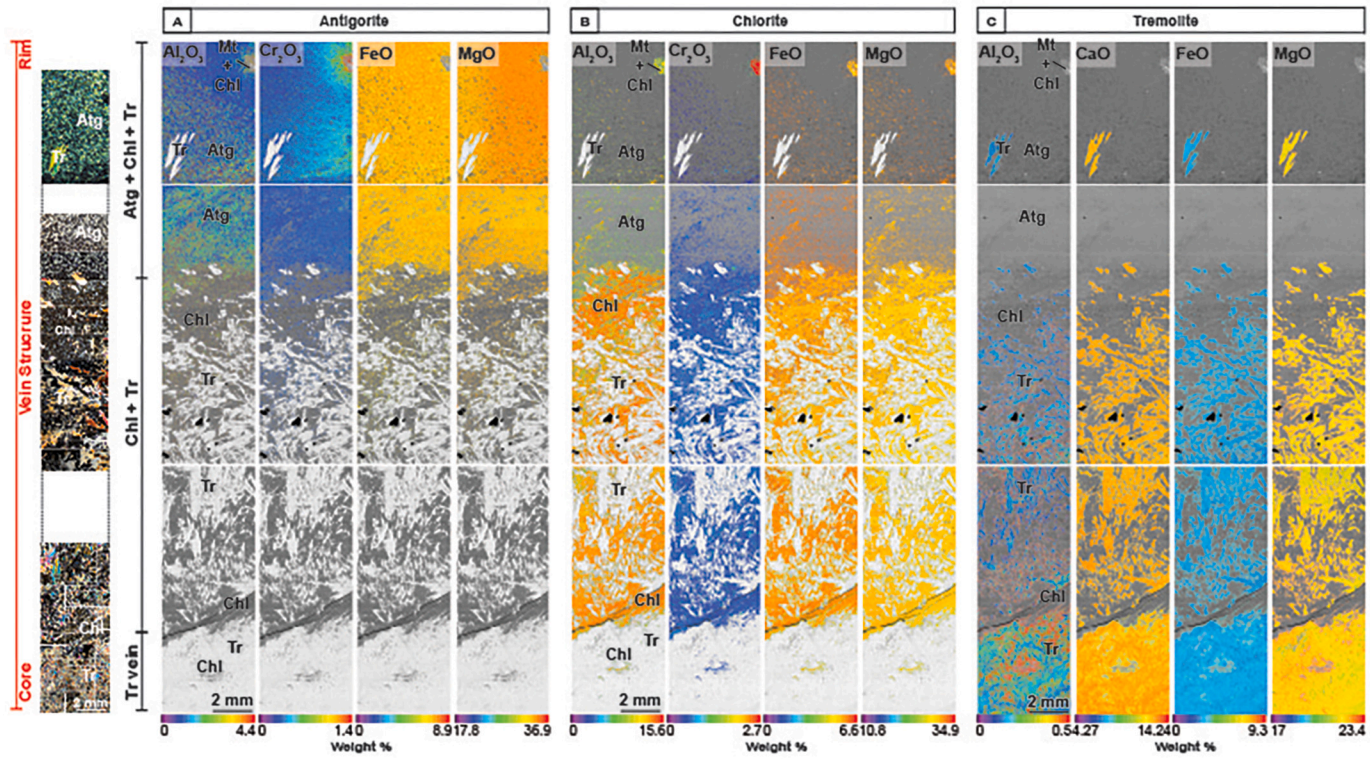

Fig. 4. Composite Al_2O_3, Cr_2O_3, FeO, MgO and CaO wt% images (calculated from X-ray maps; see text for procedure) corresponding to a cross-section of the vein structure (top is wall-rock and bottom is the center of the vein). The images were processed to show the minerals of interest (antigorite, chlorite and tremolite) set in a gray-scaled base corresponding to the BSE image that shows the basic textural features across the vein structure. Left-side images correspond to plane-polarized optical photomicrographs (crossed polars) of the scanned domains.

the Atg + Chl + Tr and Chl + Tr domains: matrix chlorite is poorer in Cr (0.02–0.15 pfu) than in high-Cr chlorite (0.19–0.62 pfu) related to small crystals of magnetite which evidence the former local presence of chromian spinel in these domains (Fig. 4B). In the Atg + Chl + Tr domain matrix chlorite has lower Al content (3.09–3.18 pfu) than in the Chl + Tr domain (up to 3.30 pfu, Fig. 2S; Table 3S) and Al and Cr show negative correlation in all domains (Fig. 2S), denoting $CrAl_{-1}$ exchange.

Amphibole in the vein and blackwall domains is tremolite with relatively constant composition. Si ranges from 7.97 to 8.00 pfu and Mg# = 0.90–0.94 (Fig. 2S; Table 3S), while it has minor amounts of Na^B (< 0.19 pfu) and $(Na + K)^A$ (0.03 to 0.22 pfu). A subtle zoning with slightly Al-enriched and Fe-poorer cores can be appreciated in the larger crystals (Fig. 4C). Magnetite has Cr = 0.02–0.03 pfu, Ti = 0.01 pfu and Ni = 0.02–0.03 pfu (Fig. 2S). Ferrian chromite has Cr = 1.24–1.73 pfu, Ti = 0.01–0.10 pfu, Fe^{3+}# [=Fe^{3+}/(Fe^{3+}+Fe^{2+})] = 0.11–0.34 and negligible amount of Al = 0.01–0.02 pfu (Fig. 2S; Table 3S). The compositional trend shows enrichment in Fe^{3+} and strong depletion in Al and Mg upon progressive transformation from ferrian chromite to magnetite (Fig. 2S).

7. Whole-rock composition

Major element composition discriminates well antigoritite and dolomite-bearing antigoritite (Figs. 6A to 6C). The restored mantle mineralogy of antigoritite indicates an orthopyroxene-rich harzburgitic protolith as opposed to dolomite-bearing antigoritite, which is apparently richer in clinopyroxene and olivine (Fig. 5A). Indeed, antigoritite shows higher SiO_2 (49.30–47.03 wt%) and lower MgO (42.13–41.36 wt %) and CaO (0.03–0.01) than dolomite-bearing antigoritite (SiO_2 = 46.09–45.02 wt%, MgO = 43.83–42.27 wt% and CaO = 1.04–0.56 wt%, anhydrous basis; Fig. 5 and Table 3S), but both types of rock have similar Al_2O_3 and FeO contents (Table 3S). This points to MgO-CaO gain and SiO_2 loss during local carbonation associated with serpentinization, making invalid the restored mantle mineralogy of the dolomite-bearing antigorite samples shown in Fig. 5A.

In agreement with the behavior of major elements, chondrite

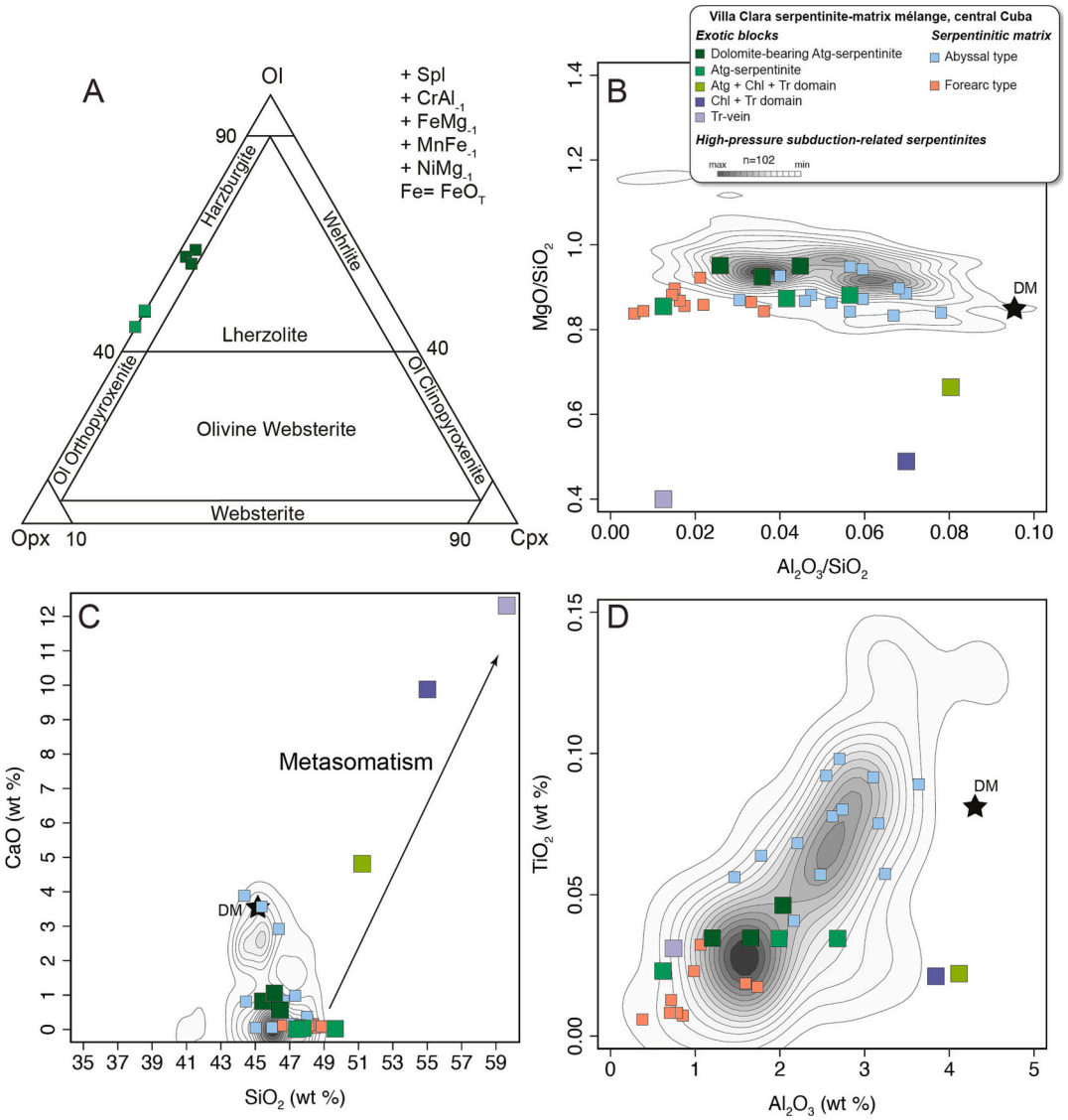

Fig. 5. Whole rock composition of antigoritites. A) Oxi-equivalent Ol-Cpx-Opx proportions of studied samples in the classification scheme of ultramafic rocks of (Le Maitre et al., 2005) (see text and Garcia-Casco et al., 2020 for justification and details of the calculation). Note that dolomite-bearing antigoritite samples fall away the Ol-Opx tie-line indicating dolomite addition. B) MgO/SiO_2 vs. Al_2O_3/SiO_2 wt%. C) CaO wt% vs SiO_2 wt%. D) TiO_2 wt% vs. Al_2O_3 wt% diagrams. Other samples correspond to abyssal- and forearc-related lizardite-serpentinites from the VCSM (Butjosa et al., 2022). Bivariate kernel density estimations (Baum, 2005) of compiled compositions from worldwide high-pressure subduction-related serpentinites (Deschamps et al., 2013) and the estimated composition of depleted mantle (DM) (Salters and Stracke, 2004) are plotted for reference. All data are in an anhydrous basis.

normalized Rare Earth Elements (REE) patterns of antigoritite and dolomite-bearing antigoritite are contrasted, pointing to either significant change in chemical composition during carbonation associated with serpentinization and/or contrasted initial composition. Antigoritite is enriched in light-REE (LREE; $La_N/Sm_N \approx 1.74–2.74$; Fig. 6A) relative to dolomite-bearing antigoritite ($La_N/Sm_N = 0.64–1.74$), showing flat patterns and slightly negative to absent Eu-anomaly ($Eu/Eu^* \approx 0.78–1.04$) while dolomite-bearing antigoritite is progressively enriched in heavy-REE (HREE; $Sm_N/Lu_N = 0.23–0.36$) and show negative Eu-anomaly ($Eu/Eu^* = 0.63–0.85$) (Fig. 6A).

As would be expected, the major element composition of blackwall domains and Tr-vein are richer in SiO_2, Al_2O_3 and CaO and poorer in MgO and FeO than the host antigoritite (Figs. 6B and C, Table 3S), but these components increase (SiO_2 and CaO) and decrease (Al_2O_3, FeO and MgO) from antigoritite through the Atg + Chl + Tr domain and the Chl + Tr domain to the Tr-vein (Table 3S). All blackwall domains and the vein are depleted in LREE and enriched in MREE and HREE ($La_N/Sm_N = 0.26$; $Sm/Lu = 0.76$) with a marked negative Eu anomaly ($Eu/Eu^* = 0.50$; Fig. 6B).

Silicate Earth–normalized patterns of antigoritites and vein domains are similar, with positive anomalies in Cs, Th, U, Pb and Ti, and negative anomalies in Nb, Ce and Sm (Fig. 6C). Large Ion Lithophile Elements (LILE) are highly enriched in blackwall domains and vein, in particular Cs and Rb, while Pb is almost constant in all samples (Fig. 6D). High Field Strength Elements (HFSE) such as Zr, Nb and Ti have a narrow range of compositions in all rock types. Notably, Th, U, Nb, Ce and HREE concentrations increase from the antigoritite host-rock through the blackwall domains to the Tr-vein. Antigoritites have restricted composition in HFSE elements with high Ti and Yb contents comparable to abyssal and subducted serpentinites (Fig. 6E). The same relations appear in the La/Sm vs Lu diagram (Fig. 6F). Initial Nd and Sr isotopes of blackwall domain Chl + Tr and vein show quite restricted ranges of $^{143}Nd/^{144}Nd_{125\ Ma}$ (0.512420–0.512424) and $^{87}Sr/^{86}Sr_{125\ Ma}$ (0.704603–0.704939) compositions, similar to the $^{87}Sr/^{86}Sr_{125\ Ma}$ (0.704482) ratio of the host antigoritite (Fig. 7, Table 2S).

8. P-T Conditions

Due to the lack of suitable thermobarometric equilibria in the antigoritites and uncertainties concerning the (variable) H_2O-CO_2 composition of the serpentinizing fluid, metamorphic conditions were constrained by means of a pseudosection approach in the system CFMASH using the calculated bulk composition of the Atg + Chl + Tr blackwall domain (see Analytical Methods) where carbonate is not present (hence allowing the inference of a non-CO_2-bearing vein-forming fluid). The selection of this blackwall domain for thermodynamic modeling is based on its lower thermodynamic variance, as compared to other studied types of rock. In an open system, larger number of coexisting phases warrants a lesser number of freely variable chemical potentials at constant P-T (Korzhinskii, 1959); hence, the selected domain offers the possibility to constrain P-T conditions with higher precision. This procedure is correct only if the Atg + Chl + Tr domain reached local equilibrium upon development, a scenario that applies only to the final stage of development of the blackwall upon arrest of fluid infiltration (see Blackwall formation model in the Discussion section). For all these reasons, the results should be considered approximate.

The P-T field of the assemblage Atg + Chl + Tr locates at 400–550 °C at 5 kbar and shrinks at higher pressure towards lower temperature (Fig. 8). In this field, the Mg# in Tr and Mg# in Chl isopleths are near-parallel, introducing large uncertainty in intersections. Furthermore, the calculated isopleths corresponding to the observed Mg# in Tr (0.90–0.94) and Chl (0.90–0.91) do not crosscut in the P-T field of the Atg + Chl + Tr assemblage, as a likely consequence of unconstrained chemical potentials of components, non-pure-H_2O fluid composition, the lack of equilibrium, the limitations of the solution models of minerals considered and/or the simple system considered. However, it is possible to tentatively propose P-T conditions of vein formation using the P-T evolution of eclogite blocks in the VCSM, which are locally enveloped by antigoritite (Somin and Millán, 1981). The P-T path of one eclogite block located not far from the Pelo Malo block reached peak conditions of *c.* 20 kbar and *c.* 575–600 °C (Fig. 8; Garcia-Casco et al., 2002, 2006), compatible with the stability of antigorite (Fig. 8; e.g., Padrón-Navarta et al., 2012 and references therein). During decompression and cooling, this path intersects the calculated phase field of the Atg + Chl + Tr domain in the range 400–500 °C and 5–10 kbar (Fig. 8), that we consider appropriate for the formation of the vein.

9. Discussion

9.1. Nature of the harzburgitic protolith and locus of antigoritization

The interpenetrating texture between dolomite and antigorite and the presence of dolomite in diffuse networks of fractures/veins/foliations demonstrates that carbonation in dolomite-bearing antigoritite took place during deformation and (ongoing) serpentinization (Fig. 3A; see Martin et al., 2016). Enrichment in MgO and CaO in this rock is considered the result of infiltration of a CaO-MgO bearing H_2O-CO_2 fluid that favored the precipitation of dolomite. In this process, compositional changes likely affected trace elements, making the composition of dolomite-bearing serpentinites not suitable for assessing the nature of its ultramafic protolith. For this reason, only antigoritite will be considered here.

Anomalies in fluid mobile elements (such as Cs, Ba, Pb, U and Sr; Fig. 6C) in antigoritite evidence protolith geochemical alteration during antigoritization. This process can take place in a shallow oceanic or deep subduction settings. Seawater, that penetrates the shallow oceanic lithosphere along transform and normal faults in the oceanic environment and along near-trench bending faults promoting serpentinization at shallow depth (Cannat, 1993; Miranda and Dilek, 2010; Ranero et al., 2003), drastically influences the Sr isotopic composition of rocks as a function of the water/rock ratio (McCulloch et al., 1981), as is commonly observed in mid-ocean ridge settings (e.g., Delacour et al., 2008, see Fig. 7). Note that, because of the relatively high Sr content of seawater and the higher mobility of Sr in rocks, even a limited interaction with seawater is enough to reset the Sr isotope ratio to that of seawater (McCulloch et al., 1981). Hence, the slight enrichment in $^{87}Sr/^{86}Sr$ in antigoritite relative to depleted mantle points to a low seawater/rock ratio that would not account for the observed full antigoritization of the harzburgitic protolith (Fig. 7).

On the other hand, fluid-immobile HFSE and REE abundances compare well with abyssal/transform fault ultramafic rocks of the VCSM and other Caribbean and worldwide localities (Butjosa et al., 2022; Deschamps et al., 2011, 2012, 2013; Hattori and Guillot, 2007). Furthermore, antigoritite has Al_2O_3/SiO_2, TiO_2, REE, HFSE and LILE patterns like subducted serpentinites of abyssal and extended continental margin peridotite protoliths (Figs. 6 and 7; Deschamps et al., 2013), strengthening that serpentinization of abyssal peridotite took place at high pressure in the subduction environment. Present day examples of serpentinites affected by subduction-derived fluids in the Mariana forearc (Savov et al., 2005, Fig. 7) show $^{87}Sr/^{86}Sr$ compositions similar to the studied antigoritites, thereby pointing to interaction with slab-derived fluids. A subduction environment is indicated also by strong ductile deformational fabric as well as the exotic character of the antigoritite block relative to the enveloping low-T (< 350 °C; Evans, 2004) Lz-serpentinite matrix, as deduced by the contrasting textures (non-pseudomorfic interpenetrating vs. pseudomorphic texture), mineralogy (antigorite vs lizardite) and lack of similar tremolite veins in the latter nearby the Pelo Malo block. We hence envisage the infiltration of a fluid produced by slab devolatilization at depth in the subduction environment at the conditions of antigoritization (i.e., at higher pressure than the vein-forming event; see below and Fig. 8). Ongoing

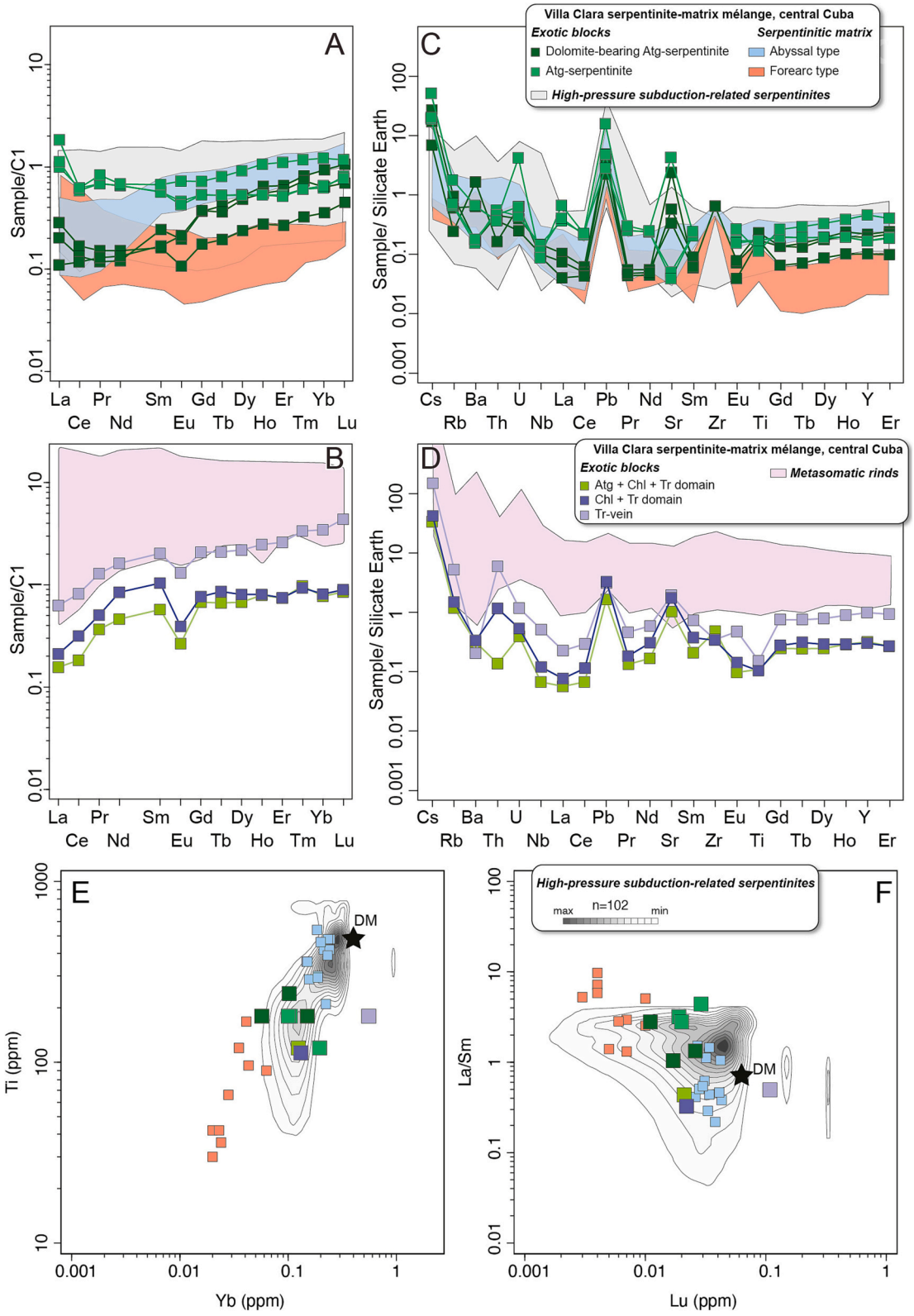

Fig. 6. Trace element composition of antigoritites and tremolite vein and associated blackwall domains. A) and C) Chondrite-normalized REE patterns, B) and D) Trace element patterns normalized to silicate earth, E) Ti vs Yb diagram, F) La/Sm vs Lu diagram. Regions corresponding to abyssal- and forearc-related lizardite-serpentinites from the VCSM (Butjosa et al., 2022) and bivariate kernel density estimation (Baum, 2005) of compiled compositions from worldwide high-pressure subduction-related serpentinites (Deschamps et al., 2013) is plotted in A) and C). The area of blueschist- and eclogite-related metasomatic rinds shown in B) and D) correspond to data from Samaná Peninsula, Dominican Republic (Sorensen et al., 1997), Alps (Angiboust et al., 2014), Santa Catalina Island (Penniston-Dorland et al., 2014; Sorensen, 1988; Sorensen and Grossman, 1989), Franciscan Complex (Saha et al., 2005; Sorensen et al., 1997; Ukar and Cloos, 2013) and New Caledonia (Taetz et al., 2016). The estimated composition of depleted mantle (DM) is from Salters and Stracke (2004). Bulk- Earth and CI-Chondrite normalizing values are after McDonough and Sun (1995).

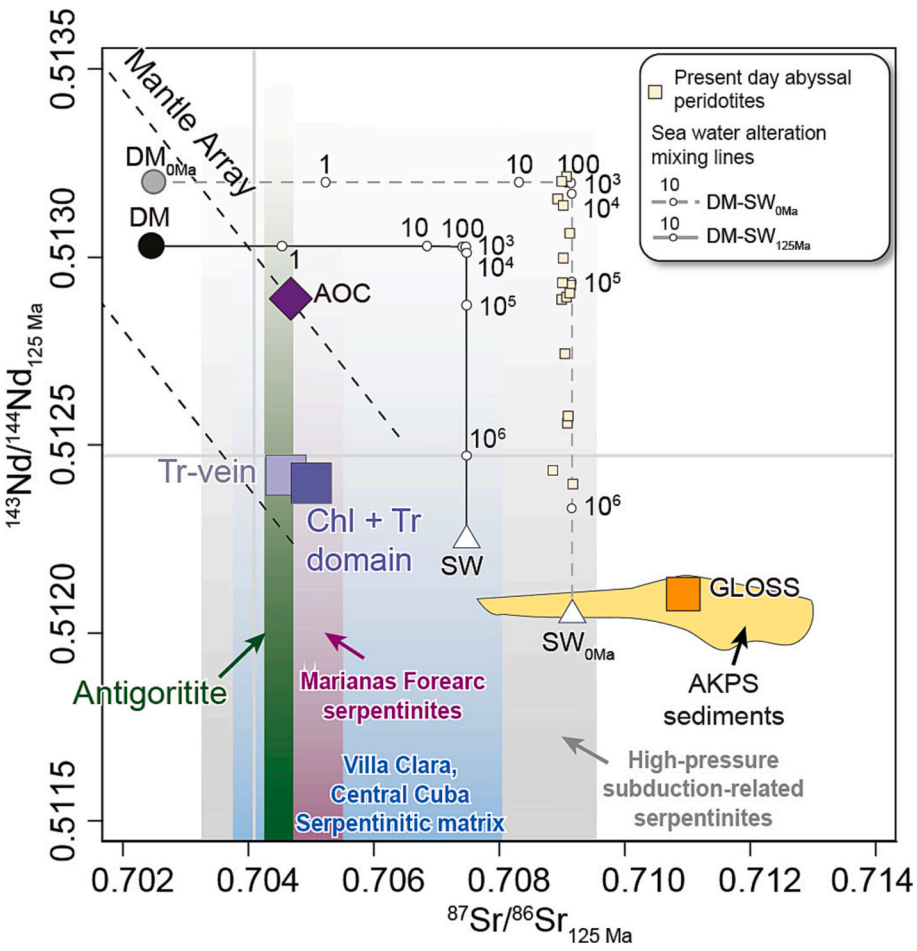

Fig. 7. $^{143}Nd/^{144}Nd$ vs $^{87}Sr/^{86}Sr$ of antigoritite, Chl + Tr domain and Tr-vein. The ranges of $^{87}Sr/^{86}Sr$ for abyssal and forearc serpentinites of the VCSM (Butjosa et al., 2022; Hattori and Guillot, 2007), Marianas forearc serpentinites (Savov et al., 2005), high-pressure subduction-related serpentinites (Cannaò et al., 2016; Marchesi et al., 2013), seawater, SW (Keto and Jacobsen, 1988; Veizer et al., 1999), Depleted Mantle, DM (Salters and Stracke, 2004), Altered Oceanic Crust, AOC (Kelley et al., 2003), Global Subducting Sediment, GLOSS (Plank, 2014) and Atlantic Cretaceous Pelagic Sediment, AKPS (Jolly et al., 2006) are plotted for comparison and reference. Seawater-DM mixing line and water/rock ratios are calculated following the equations of McCulloch et al. (1981). Data are age-corrected at the c. 125 Ma eclogitic metamorphic peak event in the VCSM (Garcia-Casco et al., 2002, 2006) with the exception of abyssal samples (small yellow squares) of Delacour et al. (2008). (For interpretation of the references to colour in this figure legend, the reader is referred to the web version of this article.)

deformation of the Pelo Malo antigoritite most likely favored porous flow of fluid that was locally channeled along relatively defuse vein networks where dolomite-bearing antigoritite locally formed (Fig. 2B). Tremolite is not present in antigoritite far from the vein networks, pointing to contrasting intervening fluids and P-T conditions during the serpentinization and vein formation events.

9.2. Origin of the vein-forming fluids

The major and trace element compositions of the vein and blackwall domains, and the metasomatic domains developed upon fluid-antigoritite reaction, clearly indicate that the infiltrated fluid was not in equilibrium with antigoritite, implying an external source for the vein-forming fluid. Also, as far as the Sr and Nd isotopic ratios of blackwall and tremolite vein do not correspond to the isotopic ratios of depleted mantle ($^{143}Nd/^{144}Nd$ is depleted and $^{87}Sr/^{86}Sr$ enriched; Fig. 7) and the Sr isotopic ratios are well below the value of 125 Ma seawater (0.707480, Veizer et al., 1999), neither seawater nor fluids evolved from subducted strongly-seawater-altered ultramafic rocks are agents associated with vein formation (Fig. 7). Instead, the isotopic relations point to the contribution of fluids evolved from subducted sediment, altered oceanic crust or their mixtures, common sources of fluids in subduction zones. As shown in Fig. 7, a slab fluid made up of variable proportions of fluids derived from subducted sediment and, probably to a lesser extent, altered oceanic crust and can satisfactorily explain the isotopic composition of the vein after interaction with a slightly seawater-serpentinized peridotite ($^{87}Sr/^{86}Sr$ corresponding to a water/rock ratio <1). That antigoritites, Tr-vein and Chl + Tr blackwall domain have similar Sr isotopic signatures (Fig. 7) pointing to a general slab-derived Sr-isotopic overprint during the vein-forming event.

The evidence provided by isotope ratios that the Pelo Malo antigoritites and vein domains formed by infiltration of fluids evolved from the slab is strengthened by the trace element composition of these rocks (Figs. 7 and 8). However, the mineral assemblages of the metasomatic domains indicate antigoritite-fluid reaction after antigoritization and ductile deformation. The brittle structures formed when a fluid was injected at ca. 15–30 km depth (5–10 kbar; Fig. 8) during the exhumation of the channel after migration from deeper parts of the subduction system. Infiltration was likely triggered by hydrofracturing, implying pressurized fluid injected from depth (Angiboust et al., 2014, 2021a, 2021b; Muñoz-Montecinos et al., 2020, 2021a, 2021b; Padrón-Navarta et al., 2010; Soret et al., 2016). The veined structure in antigoritite is hence evidence of pathways for deep-seated fluids at intermediate depth in the subduction channel.

9.3. Blackwall formation model

The vein-forming fluid contained dissolved Si, Ca, Al, Mg and Fe, for all these elements form part of the tremolite vein and adjacent blackwall. The reaction of such a fluid with the Ca-poor antigoritite formed two distinct blackwall metasomatic domains. The mineral assemblages of the domains and the composition of antigorite and chlorite (with progressive compositional changes across the composite vein structure, Fig. 4) clearly indicate changes in bulk rock composition of the wall-rock upon the progress of metasomatic reactions. A model of domain formation in the $CaO\text{-}FeO\text{-}MgO\text{-}Al_2O_3\text{-}SiO_2\text{-}H_2O$ system is illustrated in the phase-diagram of Fig. 9. This diagram is constructed in molar proportions of the indicated species after projection from tremolite

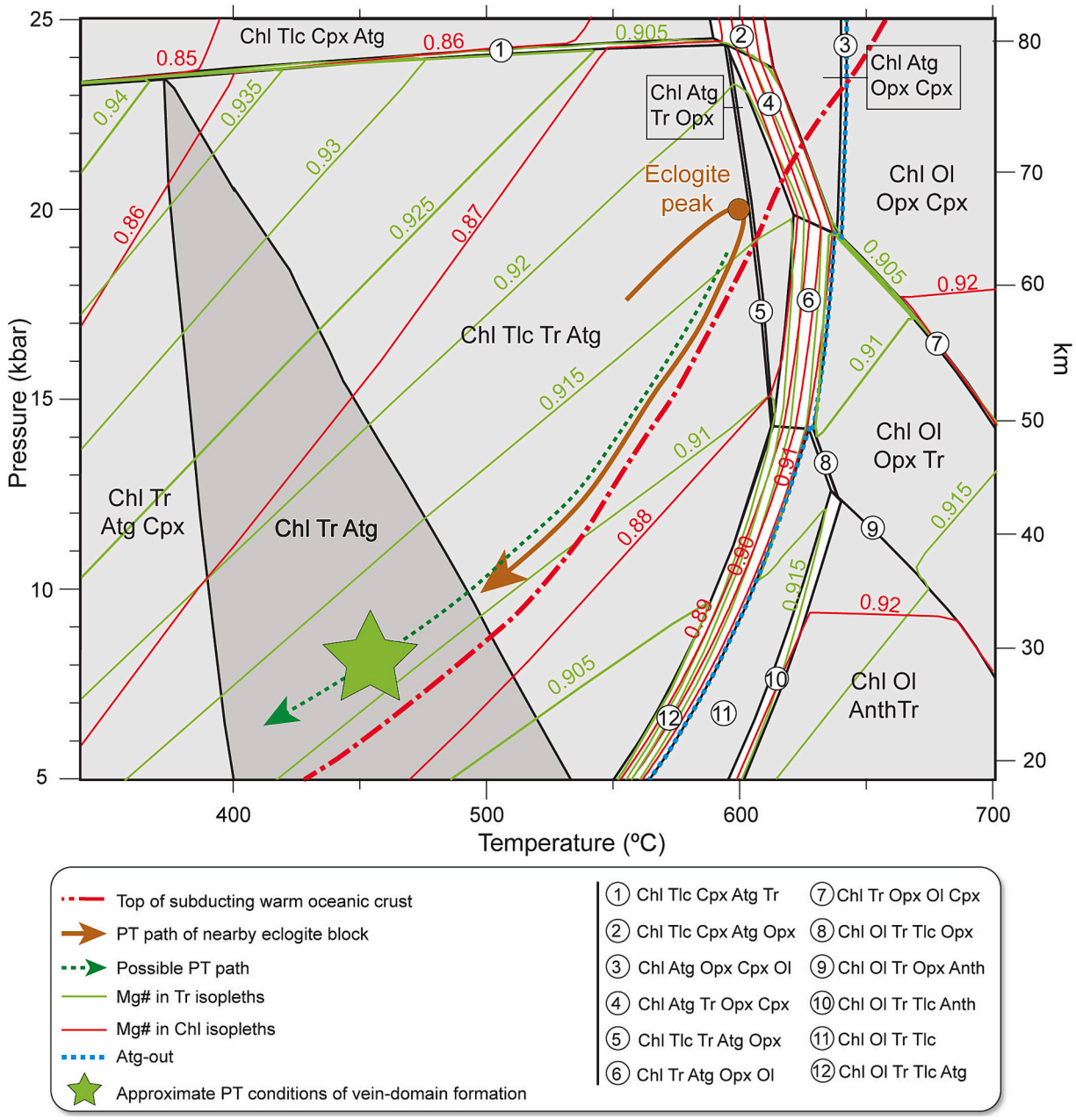

Fig. 8. Calculated P-T equilibrium phase diagram (pseudosection) for the Atg + Chl + Tr metasomatic domain in the system CFMASH (4.13 CaO wt%, 5.49 FeO wt%, 29.13 MgO wt%, 9.31 Al_2O_3 wt%, 41.00 SiO_2 wt%, H_2O in excess; see Analytical Methods). Brown-solid line represents the P-T path of a nearby eclogite block from the VCSM (Garcia-Casco et al., 2002, 2006). The thermal gradient of the top of subducting warm oceanic crust (Peacock and Wang, 1999) is plotted for reference. Blue dotted line indicates the upper thermal limit of antigorite field. Green star is the estimated P-T conditions of vein injection and formation of blackwall domain Atg + Chl + Tr along the potential exhumation path of the antigoritite block. Abbreviations: Chl, Chlorite; Atg, Antigorite; Tr, Tremolite; Tlc, Talc; Ol, Olivine; Cpx, Clinopyroxene; Opx, Orthopyroxene; Anth, Anthophyllite. The highest thermodynamic variance (F = 4) is represented by the darkest gray field assemblages and the lowest variance (F = 2) by white fields. (For interpretation of the references to colour in this figure legend, the reader is referred to the web version of this article.)

(average) and exchange vectors as indicated in the figure. Note that this projection implies that all the depicted phase assemblages contain tremolite. The projection is therefore not valid for antigoritite, but this is only a minor violation of thermodynamic rules compared to unconstrained complexities of the natural process. Among these, the unknown composition of the reacting fluid is the most important. Henceforth, the phase relations involving the Si-Al-Mg-Fe-Ca fluid illustrated in Fig. 9A are only schematic.

We first consider a "static" model for blackwall formation in which the composition of the Si-Al-Mg-Fe-Ca fluid is constant upon reaction progress. In the diagram of Fig. 9A, this scenario is illustrated by the line that joins the bulk composition of antigoritite (in the Atg-Chl tie-line, close to Atg) with the external Si-Al-Mg-Fe-Ca fluid. The topology illustrated in the diagram shows that along this line, i.e., as a function of fluid/rock ratio, two assemblages are possible, Chl + Tr + Fluid and Atg + Chl + Tr + Fluid at higher and lower fluid/rock ratios, respectively. This conceptual model fits with observations, as both theoretical assemblages correspond to the observed metasomatic domains, Chl + Tr adjacent to the vein and Atg + Chl + Tr closer to antigoritite. Furthermore, for mass-balance (i.e., reaction progress consumes fluid) and geometrical (distance from fluid at the vein fracture) reasons, higher fluid/rock ratios are expected in the Chl + Tr domain adjacent to the

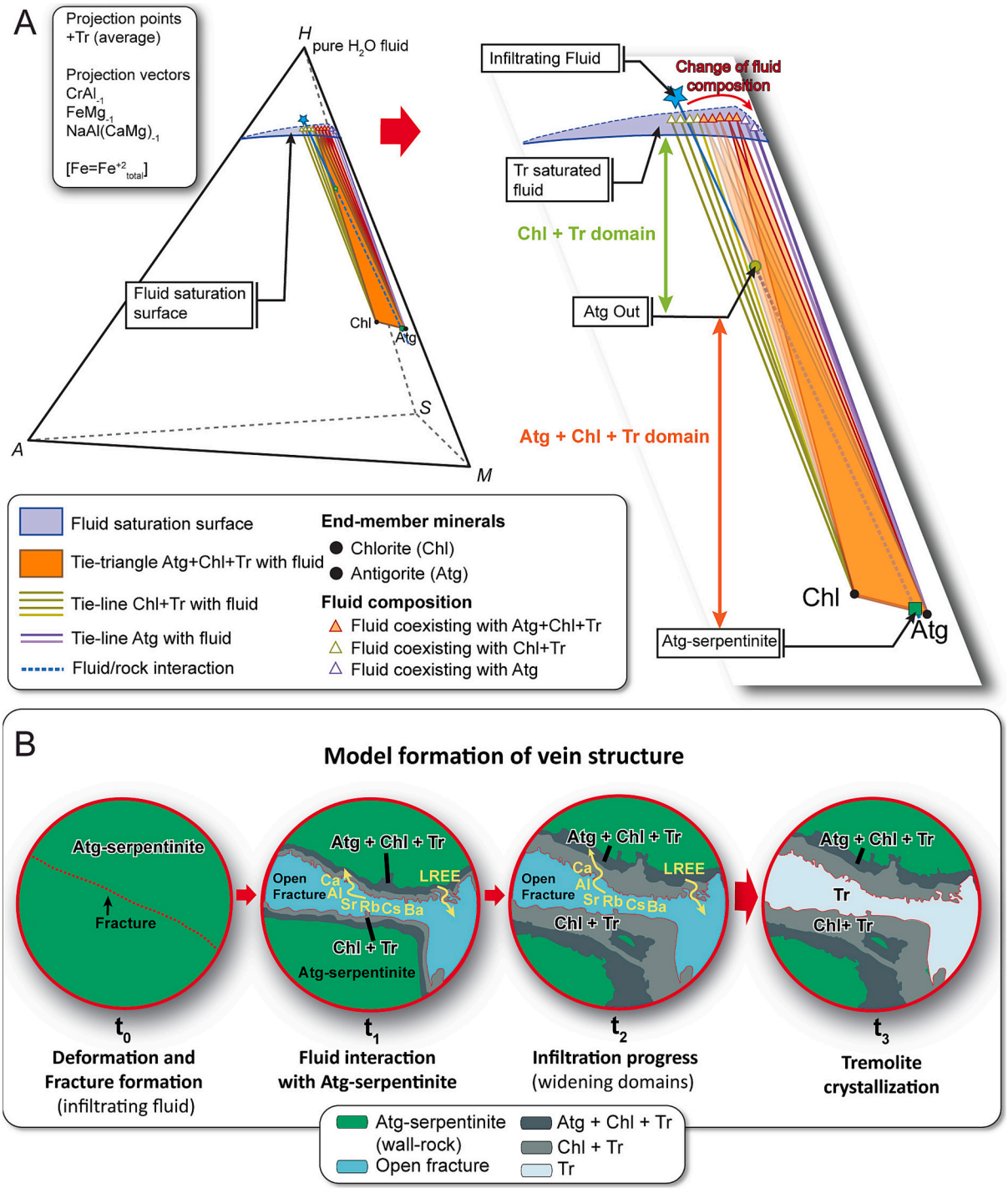

Fig. 9. Model of blackwall assemblage formation. A) Phase diagram in the MASH system showing phase relations and metasomatic zone development. All relations involving the composition of the fluid are hypothetical. The diagram is projected from Tr (average) and exchange vectors. Green tie-lines and orange tie-triangles correspond to the fields of Chl + Tr + Fluid and Atg + Chl + Tr + Fluid, respectively. Note that infiltration of fluid (blue star) in antigoritite (Atg + Chl, green square) would drive the bulk composition towards the fluid, with the development of the indicated assemblages as a function of fluid/rock ratio. Reaction progress triggers decrease in Al (as indicated by colored triangles of fluid composition) and Ca (not shown) in the fluid. B) Vein formation events. t_0: brittle deformation likely triggered by hydrofracturing; t_1 and t_2: progressive formation of the Atg + Chl + Tr and Chl + Tr domains; t_3: tremolite crystallization in the open fracture and migration of remaining fluid out of the system. See text for details. (For interpretation of the references to colour in this figure legend, the reader is referred to the web version of this article.)

vein. In other words, metasomatic zones may form as a function of the amount of infiltrated fluid by means of a reaction of the form:

$$\text{Antigorite} + \text{Si} - \text{Al} - \text{Mg} - \text{Fe} - \text{Ca Fluid} \rightarrow \text{Chlorite} + \text{Tremolite}$$

with the inner zone extensively infiltrated up to the point of reaching total consumption of antigorite and the outer zone reaching total consumption of fluid.

Even if this "static" model of a fluid of constant composition qualitatively describes the formation of two metasomatic zones adjacent to the vein, it is not correct because the progress of metasomatic reactions

should change fluid composition. A more "dynamic" scenario is described as follows. Upon the onset of fluid infiltration, a large amount of fluid infiltrated into the region adjacent to the fracture (t1, Fig. 9B), triggering large compositional changes in the system up to the point of reaching total consumption of antigorite by means of a reaction such as:

Antigorite + Fluid 1→Chlorite + Tremolite + Fluid 2.

This represents formation of the metasomatic domain Chl + Tr. Because part of Al dissolved in the fluid is incorporated in newly formed chlorite in this domain, the reaction drives the composition of the remaining fluid (Fluid 2) towards Al-poorer composition. In the MASH diagram of Fig. 9A, this translates into the displacement of the composition of the remaining fluid away from the A apex within the fluid saturation surface (Fig. 9A, green triangles: fluid coexisting with Chl + Tr domain). For similar arguments involving Ca and tremolite, Fluid 2 would be poorer in Ca (not shown). Upon infiltration further into the wall-rock of such a remaining Ca-Al-poorer fluid, fluid-consuming metasomatic reactions such as:

Antigorite + Fluid 2→Chlorite + Tremolite + Fluid 3.

would form an outer rim of Atg + Chl + Tr, as expected for topological relations (Fig. 9A). This process would drive the composition of fluid towards still poorer Ca-Al-compositions (Fluid 3, Fig. 9A orange triangles: fluid coexisting with Atg + Chl + Tr). The progressive decrease in Ca and Al in the fluid upon reaction progress would eventually reach compositions in equilibrium with antigorite and chlorite only (i.e., with antigoritite at the reaction front), preventing further formation of tremolite and arresting metasomatic transformations irrespective of the fluid/rock ratio.

The "static" and "dynamic" scenarios involve a single instantaneous batch of infiltrated fluid. Yet in an even more dynamic scenario, continuous progress of infiltration of the external Ca-Fe-Mg-Al-Si fluid would trigger progressive consumption of antigorite from the earlier formed Atg + Chl + Tr domain and displacement of the reaction front away the vein, in all cases causing widening of the two metasomatic domains until cessation of fluid infiltration (t2 in Fig. 9B; cf. Tarling et al., 2019). Finally, tremolite precipitation formed the vein (t3, in Fig. 9B), while the remaining fluid continued to flow away along propagating fractures in the subduction channel.

9.4. Exchange of matter

Once arrived to the vein system, a continuous fluid phase distributed from the vein to the wall-rock via interconnected grain boundaries and brittle (micro-) fractures (Angiboust et al., 2012, 2021b; Muñoz-Montecinos et al., 2021a, 2021b; Plümper et al., 2017). This scenario allows not only the transfer of matter from the vein fluid towards the wall-rock by means of fluid advection, but also the potential transfer of matter from the blackwall to the vein fluid by means of diffusion in the pore fluid. Fig. 10 shows the composition of metasomatic zones normalized to antigoritite wall-rock. As expected, metasomatic domain Atg + Chl + Tr is slightly less influenced by the fluid than the inner and more intensely fluxed Chl + Tr domain. Both domains, however, are strongly enriched in CaO and Sr, as a consequence of tremolite crystallization in the domains. Subtler enrichments are observed in Al_2O_3 (chlorite formation), while FeO and MgO are slightly depleted. LILE show variable behavior, with slightly enriched Rb, Cs and Ba and depletion in U and Pb (Th is uncertain). A similar contrasted behavior is observed in HFSE, with enrichment in Y and depletion in Ti, Hf and Nb (the latter observed in one domain). LREE are depleted (La, Ce, Pr), while MREE and HREE are moderately to slightly enriched (except Lu, which appears unchanged, and Eu, which shows modest depletion). This contrasting behavior

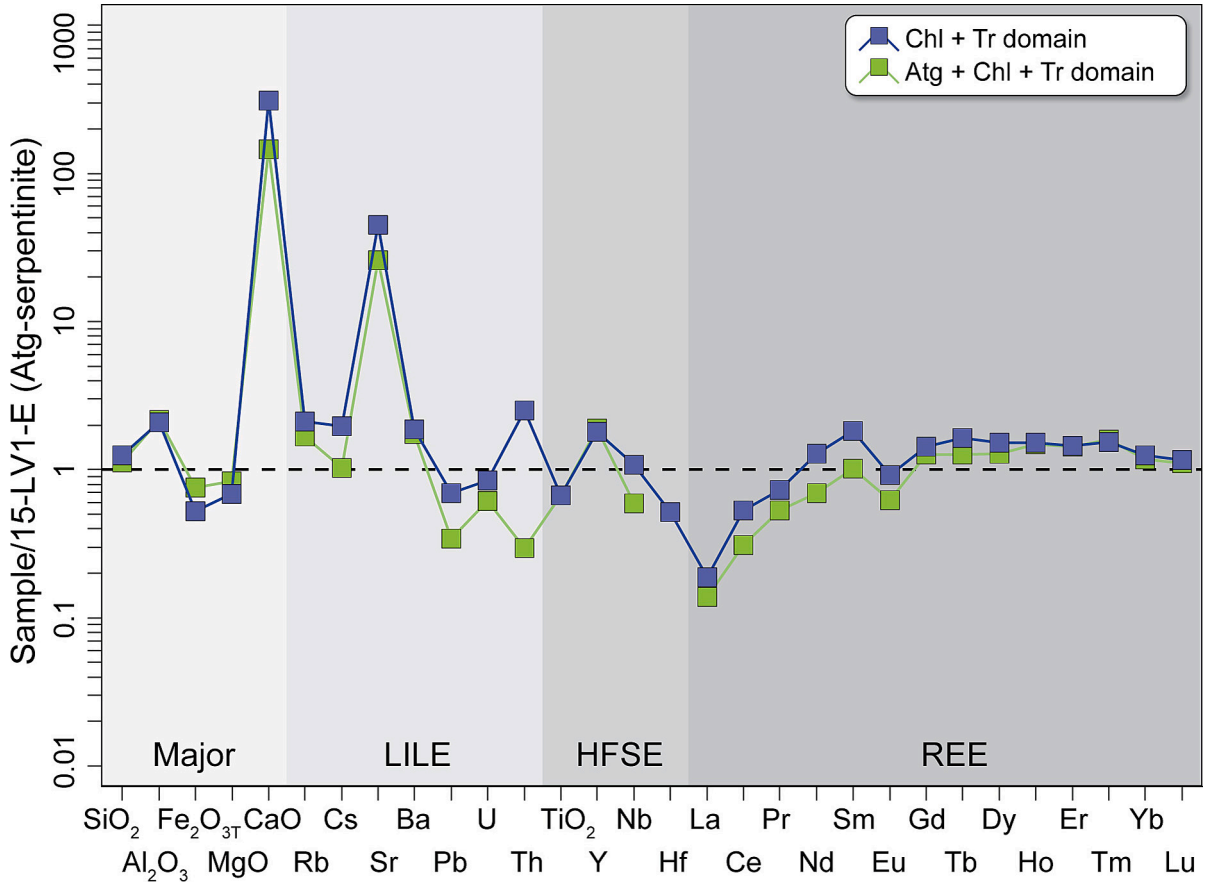

Fig. 10. Concentration of major elements, LILE, HFSE and REE of Atg + Chl + Tr and Chl + Tr domains normalized to wall-rock antigoritite (sample:15-LV-1E).

indicates that the fluid was rich in LILE and perhaps also in MREE and HREE, but it also points to further enrichment in LREE and some HFSE during blackwall formation, suggesting both advection of matter from fluid to the wall-rock and pore fluid diffusion of the latter elements towards the vein fluid. The contrasting behavior of elements is controlled, mostly, by their compatible/incompatible behavior in coexisting minerals at the temperature and pressure conditions of blackwall formation. Available experimental data for element fractionation and transport in hydrous fluids (Adam et al., 2014) indicate that LREE in amphibole are incompatible and tend to be fractionated in the fluid, while LILE are compatible and are incorporated into amphibole, in agreement with our observations and inferences.

The observed concentration of elements in the blackwall contrasts with much stronger enrichments in LILE, HFSE and REE observed in metasomatic blackwalls associated with blueschist and eclogite blocks in subduction zone environments (Figs. 7B and D), which typically contain HFSE-rich minerals (e.g., rutile, titanite, apatite, not present in the studied metasomatic domains) (Angiboust et al., 2014; Cárdenas-Párraga et al., 2021; John et al., 2008; Penniston-Dorland et al., 2012, 2014; Saha et al., 2005; Sorensen, 1988; Sorensen et al., 1997; Sorensen and Grossman, 1989; Taetz et al., 2016; Ukar and Cloos, 2013). Besides variably enriched (hence, variable sourced) fluids may explain to some extent these differences, they are primarily explained by the contrasted chemical composition of intervening rocks, with mafic blueschist- and eclogite-related blackwalls being strongly affected by the composition of the reacting protolith as compared to the LILE-, HFSE- and REE-contents of antigoritite.

As in other case-studies, our study highlights the crucial role of fluid flow triggered by slab devolatilization in the mineralogical and geochemical transformation of deep-seated ultramafic rocks from the subduction environment. The elemental and isotopic proxies and hence reliable for tracking fluid flow, which may occur at any depth, including during the return flow of mantle fragments in the subduction channel. The ultramafic rocks constitute traps for released fluids, not only during the serpentinization process, which consumes huge amount of water, but also after serpenitinization during serpentinite-fluid interaction and development of zoned black walls. The development of reaction zones (zoned black walls) will critically be controlled by the reaction progress triggered by gradients in chemical potentials (bulk composition), as exemplified here by reactions in the simple CaO-FeO-MgO-Al_2O_3-SiO_2-H_2O system. Fluid-rock interactions are controlled, however, not only by the nature of fluids evolved from slabs, but also by the nature of the rock itself, as documented by the contrasted geochemical features of black walls developed in ultramafic rocks and around blocks of subducted mafic rocks (blueschists and eclogite).

10. Conclusions

Antigorite blocks of the VCSM represent deep subduction-related geochemically abyssal serpentinite bodies of the Caribbean realm accreted to a shallow forearc mantle characterized by low-T low-P lizardite-bearing serpentinized peridotite. As opposed to the latter, they record full serpentinization (lack mantle mineral relicts) and show heterogeneous mineral assemblages (dolomite-bearing/lacking) as a result of infiltration of H_2O-CO_2 fluid mixtures at high pressure (c. 20 kbar, based on PT estimate in enclosed mafic eclogitic bodies). Further fluid injection at a later stage, most likely triggered by brittle hydrofracturing by pressurized fluid, favored localized fluid/rock interaction that developed blackwall domains (Atg + Chl + Tr and Chl + Tr) in antigoritite wall-rock adjacent to tremolite veins. Thermodynamic calculations indicate blackwall formation in the range 400–500 °C and 5–10 kbar (15–30 km) during exhumation in the subduction channel after migration from greater depth. Upon infiltration, the fluid/rock ratio varied across the metasomatic blackwall and the fluid changed composition towards Al- and Ca-poorer compositions outward the vein. The observed exchange of matter from the tremolite vein through the blackwall domains towards the antigoritite wall-rock allows characterizing the metasomatic fluid as rich in Ca, Al and LILE (mostly Sr, Rb, Cs and Ba). Sr and Nd isotope systematics indicate mixtures of fluid sourced from subducted sediment and, probably to a lesser extent, altered oceanic crust. Similar isotopic and trace element composition of vein domains, Tr-vein and antigoritite suggests similar sources of fluids that first infiltrated in a more diffuse manner, triggering generalized serpentinization at depth in the antigorite stability field during ductile deformation, and were latter injected at shallower depth forming brittle hydrofracturing structures.

Supplementary data to this article can be found online at https://doi.org/10.1016/j.lithos.2022.106973.

Declaration of Competing Interest

The authors declare the following financial interests/personal relationships which may be considered as potential competing interests: Joaquin Proenza, Antonio Garcia-Casco reports financial support was provided by Spain Ministry of Science and Innovation (MICINN PID2019-105625RB-C21). Aitor Cambeses reports financial support was provided by Government of Andalusia (P20_00550). Lidia Butjosa reports was provided by Government of Catalonia (SGR 2014–1661).

Acknowledgments

We thank one anonymous reviewer and Enrico Cannaò for the thorough revision of the manuscript and for their insightful comments. Cecile Prigent is thanked for her editorial handling and constructive comments. This research was funded by projects MICINN PID2019-105625RB-C21 (co-funded by Fondo Europeo de Desarrollo Regional, FEDER), Junta de Andalucía P20_00550, Catalonian project SGR 2014-1661 and the University of Granada. LD acknowledges PhD grant BES-2013-063205 of the Spanish Ministry of Economy and Competitiveness and scholarship of Fundació Universitària Agustí Pedro i Pons. Funding for open access charge: Universidad de Granada / CBUA

References

Adam, J., Locmelis, M., Afonso, J.C., Rushmer, T., Fiorentini, M.L., 2014. The capacity of hydrous fluids to transport and fractionate incompatible elements and metals within the Earth's mantle. Geochemistry, Geophys. Geosystems 15, 2241–2253. https://doi.org/10.1002/2013GC005199.

Ague, J.J., 2017. Element mobility during regional metamorphism in crustal and subduction zone environments with a focus on the rare earth elements (REE). Am. Mineral. 102, 1796–1821. https://doi.org/10.2138/AM-2017-6130.

Ague, J.J., Nicolescu, S., 2014. Carbon dioxide released from subduction zones by fluid-mediated reactions. Nat. Geosci. 7, 355–360. https://doi.org/10.1038/NGEO2143.

Alt, J.C., Schwarzenbach, E.M., Früh-Green, G.L., Shanks, W.C., Bernasconi, S.M., Garrido, C.J., Crispini, L., Gaggero, L., Padrón-Navarta, J.A., Marchesi, C., 2013. The role of serpentinites in cycling of carbon and sulfur: seafloor serpentinization and subduction metamorphism. Lithos 178, 40–54. https://doi.org/10.1016/J.LITHOS.2012.12.006.

Álvarez-Sánchez, H., Bernal-Rodríguez, L.R., 2015. Los mélanges Santa Clara y descanso del cinturón ofiolítico de Cuba central. In: Memorias, Trabajos y Resúmenes, VI Convención Cubana de Ciencias de La Tierra (Geociencias' 2015). Sociedad Cubana de Geología, La Habana.

Álvarez-Sánchez, H., Millán, G., Mainegra, V., Bernal-Rodríguez, L.R., Ando, J., 1991. Significado geotectónico de las rocas eclogíticas de Cuba central. In: 13 Caribbean Geological Congress. Pinar Del Rio p. Unpublished.

Angiboust, S., Wolf, S., Burov, E., Agard, P., Yamato, P., 2012. Effect of fluid circulation on subduction interface tectonic processes: Insights from thermo-mechanical numerical modelling. Earth Planet. Sci. Lett. 357–358, 238–248. https://doi.org/10.1016/j.epsl.2012.09.012.

Angiboust, S., Pettke, T., De Hoog, J.C.M., Caron, B., Oncken, O., 2014. Channelized fluid flow and eclogite-facies metasomatism along the subduction shear zone. J. Petrol. 55, 883–916. https://doi.org/10.1093/petrology/egu010.

Angiboust, S., Yamato, P., Hertgen, S., Hyppolito, T., Bebout, G.E., Morales, L., 2017. Fluid pathways and high-P metasomatism in a subducted continental slice (Mt. Emilius klippe, W. Alps). J. Metamorph. Geol. 35, 471–492. https://doi.org/10.1111/JMG.12241.

Angiboust, S., Glodny, J., Cambeses, A., Raimondo, T., Monié, P., Popov, M., Garcia-Casco, A., 2021a. Drainage of subduction interface fluids into the forearc mantle evidenced by a pristine jadeitite network (Polar Urals). J. Metamorph. Geol. 39, 473–500. https://doi.org/10.1111/jmg.12570.

Angiboust, S., Muñoz-Montecinos, J., Cambeses, A., Raimondo, T., Deldicque, D., Garcia-Casco, A., 2021b. Jolts in the Jade factory: a route for subduction fluids and their implications for mantle wedge seismicity. Earth-Science Rev. 220, 103720 https://doi.org/10.1016/j.earscirev.2021.103720.

Auzende, A.-L., Devouard, B., Guillot, S. Phane, Daniel, I., Baronnet, A., Lardeaux, J.-M., 2002. Serpentinites from Central Cuba: petrology and HRTEM study. Eur. J. Mineral. 14, 905–914. https://doi.org/10.1127/0935-1221/2002/0014-0905.

Baum, C.F., 2005. Stata: the language of choice for time-series analysis? Stata J. 5, 46–63. https://doi.org/10.1177/1536867x0500500110.

Bebout, G.E., 1991. Field-based evidence for devolatilization in subduction zones: implications for arc magmatism. Science (80-.) 251, 413–416. https://doi.org/10.1126/science.251.4992.413.

Bebout, G.E., 2007. Metamorphic chemical geodynamics of subduction zones. Earth Planet. Sci. Lett. 260, 373–393. https://doi.org/10.1016/j.epsl.2007.05.050.

Bebout, G.E., 2014. Chemical and isotopic cycling in subduction zones. In: Treatise on Geochemistry: Second Edition., pp. 703–747. https://doi.org/10.1016/B978-0-08-095975-7.00322-3.

Bebout, G.E., Penniston-Dorland, S.C., 2016. Fluid and mass transfer at subduction interfaces-the field metamorphic record. Lithos. https://doi.org/10.1016/j.lithos.2015.10.007.

Beinlich, A., Klemd, R., John, T., Gao, J., 2010. Trace-element mobilization during Ca-metasomatism along a major fluid conduit: eclogitization of blueschist as a consequence of fluid-rock interaction. Geochim. Cosmochim. Acta 74, 1892–1922. https://doi.org/10.1016/J.GCA.2009.12.011.

Bence, A.E., Albee, A.L., 1968. Empirical correction factors for the electron microanalysis of silicates and oxides. J. Geol. 76, 382–403. https://doi.org/10.1086/627339.

Blanco-Quintero, I.F., Garcia-Casco, A., Rojas-Agramonte, Y., Antonio, R.-V., Lázaro, C., Iturralde-Vinent, M.A., 2010. Metamorphic evolution of subducted hot oceanic crust (La Corea Mélange, Cuba). Am. J. Sci. 310, 889–915. https://doi.org/10.2475/11.2010.01.

Blanco-Quintero, I.F., Garcia-Casco, A., Gerya, T.V., 2011a. Tectonic blocks in serpentinite mélange (Eastern Cuba) reveal large-scale convective flow of the subduction channel. Geology 39, 79–82. https://doi.org/10.1130/G31494.1.

Blanco-Quintero, I.F., Gerya, T.V., García-Casco, A., Castro, A., 2011b. Subduction of young oceanic plates: a numerical study with application to aborted thermal-chemical plumes. Geochemistry, Geophys. Geosystems 12, Q10012. https://doi.org/10.1029/2011GC003717.

Blanco-Quintero, I.F., Lázaro, C., Garcia-Casco, A., Proenza, J.A., Rojas-Agramonte, Y., 2011c. Barium-rich fluids and melts in a subduction environment (La Corea and Sierra del Convento mélanges, eastern Cuba). Contrib. to Mineral. Petrol. 162, 395–413. https://doi.org/10.1007/s00410-010-0603-2.

Blanco-Quintero, I.F., Rojas-Agramonte, Y., Garcia-Casco, A., Kröner, A., Mertz, D.F., Lázaro, C., Blanco-Moreno, J., Renne, P.R., 2011d. Timing of subduction and exhumation in a subduction channel: evidence from slab melts from La Corea Mélange (eastern Cuba). Lithos 127, 86–100. https://doi.org/10.1016/j.lithos.2011.08.009.

Boschi, C., Dini, A., Früh-Green, G.L., Kelley, D.S., 2008. Isotopic and element exchange during serpentinization and metasomatism at the Atlantis Massif (MAR 30°N): Insights from B and Sr isotope data. Geochim. Cosmochim. Acta 72, 1801–1823. https://doi.org/10.1016/j.gca.2008.01.013.

Boschman, L.M., van Hinsbergen, D.J.J., Torsvik, T.H., Spakman, W., Pindell, J.L., 2014. Kinematic reconstruction of the caribbean region since the early jurassic. Earth-Science Rev. 138, 102–136. https://doi.org/10.1016/j.earscirev.2014.08.007.

Bouilhol, P., Burg, J.P., Bodinier, J.L., Schmidt, M.W., Bernasconi, S.M., Dawood, H., 2012. Gem olivine and calcite mineralization precipitated from subduction-derived fluids in the kohistan arc-mantle (Pakistan). Can. Mineral. 50, 1291–1304. https://doi.org/10.3749/canmin.50.5.1291.

Brady, J.B., Stout, J.H., 1980. Normalizations of thermodynamic properties and some implications for graphical and analytical problems in Petrology. Am. J. Sci. 280, 173–189.

Breeding, C.M., Ague, J.J., Bröcker, M., 2004. Fluid-metasedimentary rock interactions in subduction-zone mé lange: implications for the chemical composition of arc magmas. Geology 32, 1041–1044. https://doi.org/10.1130/G20877.1.

Butjosa, L., Cambeses, A., Proenza, J.A., Agostini, S., Iturralde-Vinent, M.A., Bernal-Rodríguez, L., Garcia-Casco, A., 2022. Relict abyssal mantle in a Caribbean forearc ophiolite (Villa Clara, central Cuba): petrogenetic and geodynamic implications. Int. Geol. Rev. under review.

Cannaò, E., Agostini, S., Scambelluri, M., Tonarini, S., Godard, M., 2015. B, Sr and Pb isotope geochemistry of high-pressure Alpine metaperidotites monitors fluid-mediated element recycling during serpentinite dehydration in subduction mélange (Cima di Gagnone, Swiss Central Alps). Geochim. Cosmochim. Acta 163, 80–100. https://doi.org/10.1016/j.gca.2015.04.024.

Cannaò, E., Scambelluri, M., Agostini, S., Tonarini, S., Godard, M., 2016. Linking serpentinite geochemistry with tectonic evolution at the subduction plate-interface: the Voltri Massif case study (Ligurian Western Alps, Italy). Geochim. Cosmochim. Acta 190, 115–133. https://doi.org/10.1016/j.gca.2016.06.034.

Cannaò, E., Scambelluri, M., Bebout, G.E., Agostini, S., Pettke, T., Godard, M., Crispini, L., 2020. Ophicarbonate evolution from seafloor to subduction and implications for deep-Earth C cycling. Chem. Geol. 546, 119626 https://doi.org/10.1016/j.chemgeo.2020.119626.

Cannat, M., 1993. Emplacement of mantle rocks in the seafloor at mid-ocean ridges. J. Geophys. Res. 98, 4163–4172. https://doi.org/10.1029/92JB02221.

Cárdenas-Párraga, J., Garcia-Casco, A., Proenza, J.A., Harlow, G.E., Blanco-Quintero, I. F., Lázaro, C., Villanova-de-Benavent, C., Núñez Cambra, K., 2017. Trace-element geochemistry of transform-fault serpentinite in high-pressure subduction mélanges (eastern Cuba): implications for subduction initiation. Int. Geol. Rev. 59, 2041–2064. https://doi.org/10.1080/00206814.2017.1308843.

Cárdenas-Párraga, J., Garcia-Casco, A., Blanco-Quintero, I.F., Rojas-Agramonte, Y., Cambra, K.N., Harlow, G.E., 2021. A highly dynamic hot hydrothermal system in the subduction environment: geochemistry and geochronology of jadeitite and associated rocks of the Sierra del Convento mélange (eastern Cuba). Am. J. Sci. 321, 822–887. https://doi.org/10.2475/06.2021.06.

Connolly, J.A.D., 1990. Multivariable phase diagrams: an algorithm based on generalized thermodynamics. Am. J. Sci. 290, 666–718. https://doi.org/10.2475/ajs.290.6.666.

Connolly, J.A.D., Galvez, M.E., 2018. Electrolytic fluid speciation by Gibbs energy minimization and implications for subduction zone mass transfer. Earth Planet. Sci. Lett. 501, 90–102. https://doi.org/10.1016/J.EPSL.2018.08.024.

Cruz-Gámez, E.M., Velasco-Tapia, F., Garcia-Casco, A., Despaigne Diaz, A.I., Lastra Rivero, J.F., Caceres Govea, D., 2016. Geochemistry of mesozoic magmatism associated with the Passive Continental Margin in the occident and center of Cuba. Bol. la Soc. Geol. Mex. 68, 443–475. https://doi.org/10.18268/BSGM2016v68n3a5.

Cruz-Orosa, I., Sàbat, F., Ramos, E., Vázquez-Taset, Y.M., 2012. Synorogenic basins of central Cuba and collision between the Caribbean and North American plates. Int. Geol. Rev. 54, 876–906. https://doi.org/10.1080/00206814.2011.585031.

Debret, B., Andreani, M., Godard, M., Nicollet, C., Schwartz, S., Lafay, R., 2013. Trace element behavior during serpentinization/de-serpentinization of an eclogitized oceanic lithosphere: a LA-ICPMS study of the Lanzo ultramafic massif (Western Alps). Chem. Geol. 357, 117–133. https://doi.org/10.1016/j.chemgeo.2013.08.025.

Delacour, A., Früh-Green, G.L., Frank, M., Gutjahr, M., Kelley, D.S., 2008. Sr- and Nd-isotope geochemistry of the Atlantis Massif (30°N, MAR): Implications for fluid fluxes and lithospheric heterogeneity. Chem. Geol. 254, 19–35. https://doi.org/10.1016/j.chemgeo.2008.05.018.

Deschamps, F., Guillot, S., Godard, M., Chauvel, C., Andreani, M., Hattori, K., 2010. In situ characterization of serpentinites from forearc mantle wedges: timing of serpentinization and behavior of fluid-mobile elements in subduction zones. Chem. Geol. 269, 262–277. https://doi.org/10.1016/j.chemgeo.2009.10.002.

Deschamps, F., Guillot, S., Godard, M., Andreani, M., Hattori, K., 2011. Serpentinites act as sponges for fluid-mobile elements in abyssal and subduction zone environments. Terra Nov. 23, 171–178. https://doi.org/10.1111/j.1365-3121.2011.00995.x.

Deschamps, F., Godard, M., Guillot, S., Chauvel, C., Andreani, M., Hattori, K., Wunder, B., France, L., 2012. Behavior of fluid-mobile elements in serpentines from abyssal to subduction environments: examples from Cuba and Dominican Republic. Chem. Geol. 312–313, 93–117. https://doi.org/10.1016/j.chemgeo.2012.04.009.

Deschamps, F., Godard, M., Guillot, S., Hattori, K., 2013. Geochemistry of subduction zone serpentinites: a review. Lithos 178, 96–127. https://doi.org/10.1016/j.lithos.2013.05.019.

Despaigne-Diaz, A.I., Garcia-Casco, A., Caceres Govea, D., Jourdan, F., Wilde, S.A., Trujillo, G.M., 2016. Twenty-five million years of subduction-accretion-exhumation during the Late Cretaceous-Tertiary in the Northwestern Caribbean: the Trinidad dome, Escambray complex, Central Cuba. Am. J. Sci. 316, 203–240. https://doi.org/10.2475/03.2016.01.

Despaigne-Diaz, A.I., Garcia-Casco, A., Caceres Govea, D., Wilde, S.A., Millán Trujillo, G., 2017. Structure and tectonic evolution of the southwestern Trinidad dome, Escambray complex, Central Cuba: insights into deformation in an accretionary wedge. Tectonophysics 717, 139–161. https://doi.org/10.1016/j.tecto.2017.07.024.

Díaz de Villalvilla, L., 1997. Caracterización geológica de las formaciones volcánicas y volcano-sedimentarias en Cuba central, provincias Cienfuegos, Villa Clara, Sancti Spiritus. In: Furrazola-Bermúdez, G., Nuñez-Cambra, K. (Eds.), Estudios Sobre Geología de Cuba. Instituto de Geología y Paleontología, Centro Nacional de la Información Geológica, La Habana, pp. 325–344.

Díaz de Villalvilla, L., Milia, I., Cruz Pacheco, M.S., Aguirre, G., 2003. Formación Los Pasos: Geología, Geoquímica y su comparación con el Caribe. In: Estudios Sobre Los Arcos Volcánicos de Cuba. Instituto de Geologia y Paleontologia, Centro Nacional de Información Geológica, La Habana, pp. 1–22.

Ducloz, C., Vuagnat, M., 1962. Apropose de l'age des serpentinites de Cuba. Arch. Sci. Phys. d'Histoire Nat. 15, 309–332.

Escuder-Viruete, J., Castillo-Carrión, M., 2016. Subduction of fore-arc crust beneath an intra-oceanic arc: the high-P Cuaba mafic gneisess and amphibolites of the Rio San Juan Complex, Dominican Republic. Lithos 262, 298–319. https://doi.org/10.1016/j.lithos.2016.07.024.

Escuder-Viruete, J., Pérez-Estaún, A., 2013. Contrasting exhumation P-T paths followed by high-P rocks in the northern Caribbean subduction-accretionary complex: insights from the structural geology, microtextures and equilibrium assemblage diagrams. Lithos 160–161. https://doi.org/10.1016/j.lithos.2012.11.028. Figure 107–144.

Escuder-Viruete, J., Friedman, R., Castillo-Carrión, M., Jabites, J., Pérez-Estaún, A., 2011a. Origin and significance of the ophiolitic high-P mélanges in the northern Caribbean convergent margin: Insights from the geochemistry and large-scale structure of the Río San Juan metamorphic complex. Lithos 127, 483–504. https://doi.org/10.1016/j.lithos.2011.09.015.

Escuder-Viruete, J., Pérez-Estaún, A., Booth-Rea, G., Valverde-Vaquero, P., 2011b. Tectonometamorphic evolution of the Samaná complex, northern Hispaniola: implications for the burial and exhumation of high-pressure rocks in a collisional accretionary wedge. Lithos 125, 190–210. https://doi.org/10.1016/j.lithos.2011.02.006.

Escuder-Viruete, J., Castillo-Carrión, M., Pérez-Estaún, A., 2014. Magmatic relationships between depleted mantle harzburgites, boninitic cumulate gabbros and subduction-related tholeiitic basalts in the Puerto Plata ophiolitic complex, Dominican Republic: Implications for the birth of the Caribbean island-arc. Lithos 196–197, 261–280. https://doi.org/10.1016/j.lithos.2014.03.013.

Escuder-Viruete, J., Suárez-Rodríguez, Á., Gabites, J., Pérez-Estaún, A., 2016. The Imbert Formation of northern Hispaniola: a tectono-sedimentary record of arc-continent

collision and ophiolite emplacement in the northern Caribbean subduction-accretionary prism. Solid Earth 7, 11–36. https://doi.org/10.5194/se-7-11-2016.
Evans, B.W., 2004. The serpentinite multisystem revisited: chrysotile is metastable. Int. Geol. Rev. 46, 479–506. https://doi.org/10.2747/0020-6814.46.6.479.
Fisher, G.W., 1989. Matrix analysis of metamorphic mineral assemblages and reactions. Contrib. to Mineral. Petrol. 102, 69–77. https://doi.org/10.1007/BF01160191.
Fisher, G.W., 1993. An improved method for algebraic analysis of metamorphic mineral assemblages. Am. Mineral. 78, 1257–1261.
García Delgado, D.E., Pérez Pérez, C., Delgado Damas, R., Díaz Otero, C., Millán, G., Furrazola, G., Díaz de Villalvilla, L., García Cadiz, I., Sukar, K., Delgado Carballo, I., Bernal, L., Pardo, M., Rojas-Agramonte, Y., Suárez Leyva, V., Duani Duarte, E., 1998. Mapa geológico de Cuba central (provincias Cienfuegos, Villa Clara y Sancti Spiritus). Escala 1, 100000.
Garcia-Casco, A., 2007. Magmatic paragonite in trondhjemites from the Sierra del Convento mélange, Cuba. Am. Mineral. 92, 1232–1237. https://doi.org/10.2138/am.2007.2598.
Garcia-Casco, A., Torres-Roldán, R.L., Millán, G., Monié, P., Schneider, J., 2002. Oscillatory zoning in eclogitic garnet and amphibole, Northern Serpentinite Melange, Cuba: a record of tectonic instability during subduction? J. Metamorph. Geol. 20, 581–598. https://doi.org/10.1046/j.1525-1314.2002.00390.x.
Garcia-Casco, A., Torres-Roldán, R.L., Iturralde-Vinent, M.A., Millán, G., Núñez Cambra, K., Lázaro, C., Rodríguez Vega, A., 2006. High pressure metamorphism of ophiolites in Cuba. Geol. Acta 4, 63–88. https://doi.org/10.1344/105.000000358.
Garcia-Casco, A., Iturralde-Vinent, M.A., Pindell, J., 2008a. Latest Cretaceous collision/accretion between the Caribbean plate and Caribeana: origin of metamorphic terranes in the greater antilles. Int. Geol. Rev. 50, 781–809. https://doi.org/10.2747/0020-6814.50.9.781.
Garcia-Casco, A., Lázaro, C., Rojas-Agramonte, Y., Kröner, A., Torres-Roldán, R.L., Núñez, K., Neubauer, F., Millán, G., Blanco-Quintero, I., 2008b. Partial melting and counterclockwise P-T path of subducted oceanic crust (Sierra del Convento Mélange, Cuba). J. Petrol. 49, 129–161. https://doi.org/10.1093/petrology/egm074.
Garcia-Casco, A., Restrepo, J.J., Correa-Martínez, A.M., Blanco-Quintero, I.F., Proenza, J. A., Weber, M., Butjosa, L., 2020. The petrologic nature of the "Medellín Dunite" revisited: an algebraic approach and proposal of a new definition of the geological body. In: Gómez, J., Pinilla-Pachon, A.O. (Eds.), The Geology of Colombia. Servicio Geológico Colombiano. Publicaciones Geológicas Especiales 36, Bogotá, pp. 45–75. https://doi.org/10.32685/pub.esp.36.2019.02.
Gilio, M., Scambelluri, M., Agostini, S., Godard, M., Peters, D., Pettke, T., 2019. Petrology and Geochemistry of serpentinites associated with the ultra-High pressure Lago di Cignana Unit (Italian Western Alps). J. Petrol. 60, 1229–1262. https://doi.org/10.1093/PETROLOGY/EGZ030.
Govindaraju, K., 1994. Compilation of working values and sample description for 383 geostandards. Geostand. Newslett. 18, 1–158. https://doi.org/10.1046/j.1365-2494.1998.53202081.x-i1.
Groppo, C., Rinaudo, C., Cairo, S., Gastaldi, D., Compagnoni, R., 2006. Micro-Raman spectroscopy for a quick and reliable identification of serpentine minerals from ultramafics. Eur. J. Mineral. 18, 319–329. https://doi.org/10.1127/0935-1221/2006/0018-0319.
Hacker, B.R., 2008. H2O subduction beyond arcs. Geochemistry, Geophys. Geosystems 9, Q03001. https://doi.org/10.1029/2007GC001707.
Hall, C.M., Kesler, S.E., Russell, N., Pinero, E., Roberto Sánchez, C., Mireya Pérez, R., Moreira, J., Borges, M., 2004. Age and tectonic setting the Camagüey volcanic-intrusive arc, Cuba: Late Cretaceous extension and uplift in the Western Greater Antilles. J. Geol. 112, 521–542. https://doi.org/10.1086/422664.
Harlow, G.E., Sorensen, S.S., 2005. Jade (Nephrite and Jadeitite) and Serpentinite: Metasomatic Connections. Int. Geol. Rev. 47, 113–146. https://doi.org/10.2747/0020-6814.47.2.113.
Hart, S.R., Blusztajn, J., Dick, H.J.B., Meyer, P.S., Muehlenbachs, K., 1999. The fingerprint of seawater circulation in a 500-meter section of ocean crust gabbros. Geochim. Cosmochim. Acta 63, 4059–4080. https://doi.org/10.1016/s0016-7037(99)00309-9.
Hattori, K.H., Guillot, S., 2007. Geochemical character of serpentinites associated with high- to ultrahigh-pressure metamorphic rocks in the Alps, Cuba, and the Himalayas: Recycling of elements in subduction zones. Geochemistry, Geophys. Geosystems 8, Q09010. https://doi.org/10.1029/2007GC001594.
Hawthorne, F.C., Oberti, R., Harlow, G.E., Maresch, W.V., Martin, R.F., Schumacher, J. C., Welch, M.D., 2012. Ima report: Nomenclature of the amphibole supergroup. Am. Mineral. 97, 2031–2048. https://doi.org/10.2138/am.2012.4276.
Hermann, J., Spandler, C., Hack, A., Korsakov, A.V., 2006. Aqueous fluids and hydrous melts in high-pressure and ultra-high pressure rocks: implications for element transfer in subduction zones. Lithos 92, 399–417. https://doi.org/10.1016/J.LITHOS.2006.03.055.
Holland, T., Powell, R., 1996. Thermodynamics of order-disorder in minerals: II. Symmetric formalism applied to solid solutions. Am. Mineral. 81, 1425–1437. https://doi.org/10.2138/am-1996-11-1215.
Holland, T.J.B., Powell, R., 2011. An improved and extended internally consistent thermodynamic dataset for phases of petrological interest, involving a new equation of state for solids. J. Metamorph. Geol. 29, 333–383. https://doi.org/10.1111/j.1525-1314.2010.00923.x.
Holland, T., Baker, J., Powell, R., 1998. Mixing properties and activity-composition relationships of chlorites in the system MgO-FeO-Al2O3-SiO2-H2O. Eur. J. Mineral. 10, 395–406. https://doi.org/10.1127/ejm/10/3/0395.
Hu, H.Y., Stern, R.J., Rojas-Agramonte, Y., Garcia-Casco, A., 2022. Review of geochronologic and geochemical data of the Greater Antilles Volcanic Arc and implications for the evolution of oceanic arcs. Geochemistry, Geophys. Geosystems 23. https://doi.org/10.1029/2021gc010148 e2021GC010148.
Humphris, S.E., Thompson, G., 1978. Hydrothermal alteration of oceanic basalts by seawater. Geochim. Cosmochim. Acta 42, 107–125. https://doi.org/10.1016/0016-7037(78)90221-1.
Iturralde-Vinent, M.A., 1996. Geología de las ofiolitas de Cuba. In: Iturralde-Vinent, M.A. (Ed.), Ofiolitas y Arcos Volcánicos de Cuba. International Geological Correlation Program (IGCP) Project 364, Miami, pp. 179–189.
Iturralde-Vinent, M.A., 1998. Sinopsis de la Constitución Geológica de Cuba. Acta Geol. Hisp. 33, 9–56.
Iturralde-Vinent, M.A., Millán, G., Korpás, L., Nagy, E., Pajón, J., 1996. Geological interpretation of the Cuban K-Ar database. In: Iturralde-Vinent, M.A. (Ed.), Ofiolitas y Arcos Volcánicos de Cuba. International Geological Correlation Program (IGCP) Project 364, Miami, pp. 48–69.
Iturralde-Vinent, M.A., Otero, C.D., Garcia-Casco, A., van Hinsbergen, D.J.J., 2008. Paleogene foredeep basin deposits of north-central Cuba: A record of Arc-continent collision between the Caribbean and North American plates. Int. Geol. Rev. 50, 863–884. https://doi.org/10.2747/0020-6814.50.10.863.
Iturralde-Vinent, M.A., Garcia-Casco, A., Rojas-Agramonte, Y., Proenza, J.A., Murphy, J. B., Stern, R.J., 2016. The geology of Cuba: a brief overview and synthesis. GSA Today 26, 4–10. https://doi.org/10.1130/GSATG296A.1.
John, T., Klemd, R., Gao, J., Garbe-Schönberg, C.D., 2008. Trace-element mobilization in slabs due to non steady-state fluid-rock interaction: constraints from an eclogite-facies transport vein in blueschist (Tianshan, China). Lithos 103, 1–24. https://doi.org/10.1016/j.lithos.2007.09.005.
Jolly, W.T., Lidiak, E.G., Dickin, A.P., 2006. Cretaceous to Mid-Eocene pelagic sediment budget in Puerto Rico and the Virgin Islands (northeast Antilles Island arc). Geol. Acta 4, 35–62.
Kanchev, I., Boyanov, I., Popov, N., Cabrera, R., Goranov, A., Iolkicev, N., Kanazirski, M., Stancheva, M., 1978. Informe Geología de la Província de Las Villas. La Habana-Sofia.
Kelley, K.A., Plank, T., Ludden, J., Staudigel, H., 2003. Composition of altered oceanic crust at ODP Sites 801 and 1149. Geochemistry, Geophys. Geosystems 4, 8910. https://doi.org/10.1029/2002GC000435.
Kerr, A.C., Iturralde-Vinent, M.A., Saunders, A.D., Babbs, T.L., Tarney, J., 1999. A new plate tectonic model of the Caribbean: Implications from a geochemical reconnaissance of Cuban Mesozoic volcanic rocks. Bull. Geol. Soc. Am. 111, 1581–1599. https://doi.org/10.1130/0016-7606(1999)111<1581:ANPTMO>2.3.CO;2.
Keto, L.S., Jacobsen, S.B., 1988. Nd isotopic variations of Phanerozoic paleoceans. Earth Planet. Sci. Lett. 90, 395–410. https://doi.org/10.1016/0012-821X(88)90138-0.
King, R.L., Bebout, G.E., Moriguti, T., Nakamura, E., 2006. Elemental mixing systematics and Sr-Nd isotope geochemistry of mélange formation: obstacles to identification of fluid sources to arc volcanics. Earth Planet. Sci. Lett. 246, 288–304. https://doi.org/10.1016/j.epsl.2006.03.053.
Kodolányi, J., Pettke, T., Spandler, C., Kamber, B.S., Ling, K.G., 2012. Geochemistry of ocean floor and fore-arc serpentinites: constraints on the ultramafic input to subduction zones. J. Petrol. 53, 235–270. https://doi.org/10.1093/petrology/egr058.
Konrad-Schmolke, M., O'Brien, P.J., Zack, T., 2011. Fluid migration above a subducted slab-constraints on amount, pathways and major element mobility from partially overprinted eclogite-facies rocks (Sesia Zone, Western Alps). J. Petrol. 52, 457–486. https://doi.org/10.1093/petrology/egq087.
Korzhinskii, D.S., 1959. No TitlePhysicochemical Basis of the Analysis of the Paragenesis of Minerals. Consultants Bureau, New York.
Lafay, R., Deschamps, F., Schwartz, S., Guillot, S., Godard, M., Debret, B., Nicollet, C., 2013. High-pressure serpentinites, a trap-and-release system controlled by metamorphic conditions: example from the Piedmont zone of the western Alps. Chem. Geol. 343, 38–54. https://doi.org/10.1016/j.chemgeo.2013.02.008.
Lázaro, C., Garcia-Casco, A., 2008. Geochemical and Sr-Nd isotope signatures of pristine slab melts and their residues (Sierra del Convento mélange, eastern Cuba). Chem. Geol. 255, 120–133. https://doi.org/10.1016/J.CHEMGEO.2008.06.017.
Lázaro, C., Garcia-Casco, A., Rojas-Agramonte, Y., Kröner, A., Neubauer, F., Iturralde-Vinent, M., 2009. Fifty-five-million-year history of oceanic subduction and exhumation at the northern edge of the Caribbean plate (Sierra del Convento mélange, Cuba). J. Metamorph. Geol. 27, 19–40. https://doi.org/10.1111/j.1525-1314.2008.00800.x.
Lázaro, C., Blanco-Quintero, I.F., Marchesi, C., Bosch, D., Rojas-Agramonte, Y., Garcia-Casco, A., 2011. The imprint of subduction fluids on subducted MORB-derived melts (Sierra del Convento Mélange, Cuba). Lithos 126, 341–354. https://doi.org/10.1016/j.lithos.2011.07.011.
Lázaro, C., Blanco-Quintero, I.F., Proenza, J.A., Rojas-Agramonte, Y., Neubauer, F., Núñez-Cambra, K., Garcia-Casco, A., 2016. Petrogenesis and 40 Ar/39 Ar dating of proto-forearc crust in the Early Cretaceous Caribbean arc: the la Tinta mélange (eastern Cuba) and its easterly correlation in Hispaniola. Int. Geol. Rev. 58, 1020–1040. https://doi.org/10.1080/00206814.2015.1118647.
Le Maitre, R.W., Streckeisen, A., Zanettin, B., Le Bas, M.J., Bonin, B., Bateman, P., 2005. Igneous Rocks: A Classification and Glossary of Terms: Recommendations of the International Union of Geological Sciences Subcommission on the Systematics of Igneous Rocks. Cambridge University Press.
Lewis, J.F., Draper, G., Proenza, J.A., Espaillat, J., Jiménez, J., 2006. Ophiolite-related ultramafic rocks (serpentinites) in the Caribbean region: a review of their occurrence, composition, origin, emplacement and Ni-laterite soil formation. Geol. Acta 4, 237–263.
Lidiak, E.G., Anderson, T.H., 2015. Evolution of the Caribbean plate and origin of the Gulf of Mexico in light of plate motions accommodated by strike-slip faulting. Spec. Pap. Geol. Soc. Am. 513, 1–88. https://doi.org/10.1130/2015.2513(01).

Llanes Castro, A.I., Furnes, H., Cruz Gámez, E.M., Rodriguez, M.P., Cruz, O.L., 2018. Petrogenesis of plagiogranite and associated diorites and mafic rocks in the Habana–Matanzas ophiolites, northwestern half of central Cuba. J. Geol. Soc. Lond. 176, 992–1006. https://doi.org/10.1144/jgs2018-116.

Marchesi, C., Garrido, C.J., Padrón-Navarta, J.A., López Sánchez-Vizcaíno, V., Gómez-Pugnaire, M.T., 2013. Element mobility from seafloor serpentinization to high-pressure dehydration of antigorite in subducted serpentinite: Insights from the Cerro del Almirez ultramafic massif (southern Spain). Lithos 178, 128–142. https://doi.org/10.1016/j.lithos.2012.11.025.

Martin, C., Flores, K.E., Harlow, G.E., 2016. Boron isotopic discrimination for subduction-related serpentinites. Geology 44, 899–902. https://doi.org/10.1130/G38102.1.

McCulloch, M.T., Gregory, R.T., Wasserburg, G.J., Taylor, H.P., 1981. Sm-Nd, Rb-Sr, and 18O/16O isotopic systematics in an oceanic crustal section: evidence from the Samail ophiolite. J. Geophys. Res. 86, 2721–2735. https://doi.org/10.1029/JB086iB04p02721.

McDonough, W.F., Sun, S.S., 1995. The composition of the Earth. Chem. Geol. 120, 223–253. https://doi.org/10.1016/0009-2541(94)00140-4.

Miranda, E.A., Dilek, Y., 2010. Oceanic core complex development in modern and Ancient Oceanic Lithosphere: Gabbro-Localized versus Peridotite-Localized Detachment models. J. Geol. 118, 95–109. https://doi.org/10.1086/648460.

Molina, J.F., Poli, S., 2000. Carbonate stability and fluid composition in subducted oceanic crust: an experimental study on H2O-CO2-bearing basalts. Earth Planet. Sci. Lett. 176, 295–310. https://doi.org/10.1016/S0012-821X(00)00021-2.

Montero, P., Bea, F., 1998. Accurate determination of 87Rb/86Sr and 147Sm/144Nd ratios by inductively-coupled-plasma mass spectrometry in isotope geoscience: an alternative to isotope dilution analysis. Anal. Chim. Acta 358 (3), 227–233.

Muñoz-Montecinos, J., Angiboust, S., Cambeses, A., García-Casco, A., 2020. Multiple veining in a paleo–accretionary wedge: the metamorphic rock record of prograde dehydration and transient high pore-fluid pressures along the subduction interface (Western Series, central Chile). Geosphere 16, 765–786. https://doi.org/10.1130/ges02227.1.

Muñoz-Montecinos, J., Angiboust, S., Garcia-Casco, A., 2021a. Blueschist-facies paleo-earthquakes in a serpentinite channel (Zagros suture, Iran) enlighten seismogenesis in Mariana-type subduction margins. Earth Planet. Sci. Lett. 573, 117135 https://doi.org/10.1016/j.epsl.2021.117135.

Muñoz-Montecinos, J., Angiboust, S., Garcia-Casco, A., Glodny, J., Bebout, G., 2021b. Episodic hydrofracturing and large-scale flushing along deep subduction interfaces: Implications for fluid transfer and carbon recycling (Zagros Orogen, southeastern Iran). Chem. Geol. 571, 120173 https://doi.org/10.1016/j.chemgeo.2021.120173.

Padrón-Navarta, J.A., Tommasi, A., Garrido, C.J., Sánchez-Vizcaíno, V.L., Gómez-Pugnaire, M.T., Jabaloy, A., Vauchez, A., 2010. Fluid transfer into the wedge controlled by high-pressure hydrofracturing in the cold top-slab mantle. Earth Planet. Sci. Lett. 297, 271–286. https://doi.org/10.1016/j.epsl.2010.06.029.

Padrón-Navarta, J.A., Sánchez-Vizcaí, V.L., Garrido, C.J., Gómez-Pugnaire, M.T., 2011. Metamorphic record of high-pressure dehydration of antigorite serpentinite to chlorite harzburgite in a subduction setting (Cerro del Almirez, Nevado-Filábride complex, Southern Spain). J. Petrol. 52, 2047–2078. https://doi.org/10.1093/petrology/egr039.

Padrón-Navarta, J.A., Tommasi, A., Garrido, C.J., López Sánchez-Vizcaíno, V., 2012. Plastic deformation and development of antigorite crystal preferred orientation in high-pressure serpentinites. Earth Planet. Sci. Lett. 349–350, 75–86. https://doi.org/10.1016/j.epsl.2012.06.049.

Padrón-Navarta, J.A., Sánchez-Vizcaíno, V.L., Hermann, J., Connolly, J.A.D., Garrido, C. J., Gómez-Pugnaire, M.T., Marchesi, C., 2013. Tschermak's substitution in antigorite and consequences for phase relations and water liberation in high-grade serpentinites. Lithos 178, 186–196. https://doi.org/10.1016/j.lithos.2013.02.001.

Peacock, S.M., Wang, K., 1999. Seismic consequences of warm versus cool subduction metamorphism: examples from southwest and northeast Japan. Science (80-.) 286, 937–939. https://doi.org/10.1126/science.286.5441.937.

Penniston-Dorland, S.C., Sorensen, S.S., Ash, R.D., Khadke, S.V., 2010. Lithium isotopes as a tracer of fluids in a subduction zone mélange: Franciscan Complex, CA. Earth Planet. Sci. Lett. 292, 181–190. https://doi.org/10.1016/j.epsl.2010.01.034.

Penniston-Dorland, S.C., Bebout, G.E., Pogge von Strandmann, P.A.E., Elliott, T., Sorensen, S.S., 2012. Lithium and its isotopes as tracers of subduction zone fluids and metasomatic processes: evidence from the Catalina Schist, California, USA. Geochim. Cosmochim. Acta 77, 530–545. https://doi.org/10.1016/j.gca.2011.10.038.

Penniston-Dorland, S.C., Gorman, J.K., Bebout, G.E., Piccoli, P.M., Walker, R.J., 2014. Reaction rind formation in the Catalina Schist: deciphering a history of mechanical mixing and metasomatic alteration. Chem. Geol. 384, 47–61. https://doi.org/10.1016/j.chemgeo.2014.06.024.

Piccoli, F., Vitale Brovarone, A., Beyssac, O., Martinez, I., Ague, J.J., Chaduteau, C., 2016. Carbonation by fluid–rock interactions at high-pressure conditions: Implications for carbon cycling in subduction zones. Earth Planet. Sci. Lett. 445, 146–159. https://doi.org/10.1016/J.EPSL.2016.03.045.

Piccoli, F., Ague, J.J., Chu, X., Tian, M., Vitale Brovarone, A., 2021. Field-based evidence for intra-slab high-permeability channel formation at eclogite-facies conditions during subduction. Geochemistry, Geophys. Geosystems 22. https://doi.org/10.1029/2020GC009520 e2020GC009520.

Pindell, J., Kennan, L., 2009. Tectonic evolution of the Gulf of Mexico, Caribbean and northern South America in the mantle reference frame: an update. Geol. Soc. Spec. Publ. 328, 1–55. https://doi.org/10.1144/SP328.1.

Pindell, J., Maresch, W.V., Martens, U., Stanek, K., 2012. The Greater Antillean Arc: early cretaceous origin and proposed relationship to Central American subduction mélanges: Implications for models of Caribbean evolution. Int. Geol. Rev. https://doi.org/10.1080/00206814.2010.510008.

Plank, T., 2014. The chemical composition of subducting sediments. In: Treatise on Geochemistry: Second Edition., pp. 607–629. https://doi.org/10.1016/B978-0-08-095975-7.00319-3.

Plümper, O., John, T., Podladchikov, Y.Y., Vrijmoed, J.C., Scambelluri, M., 2017. Fluid escape from subduction zones controlled by channel-forming reactive porosity. Nat. Geosci. 10, 150–156. https://doi.org/10.1038/ngeo2865.

Proenza, J.A., Díaz-Martínez, R., Iriondo, A., Marchesi, C., Melgarejo, J.C., Gervilla, F., Garrido, C.J., Rodríguez-Vega, A., Lozano-Santacruz, R., Blanco-Moreno, J.A., 2006. Primitive Cretaceous island-arc volcanic rocks in eastern Cuba: the Téneme Formation. Geol. Acta 4, 103–121.

Ranero, C.R., Phipps Morgan, J., McIntosh, K., Relchert, C., 2003. Bending-related faulting and mantle serpentinization at the Middle America trench. Nature 425, 367–373. https://doi.org/10.1038/nature01961.

Rojas-Agramonte, Y., Kröner, A., Garcia-Casco, A., Kemp, T., Hegner, E., Pérez, M., Barth, M., Liu, D., Fonseca-Montero, A., 2010. Zircon ages, Sr-Nd-Hf isotopic compositions, and geochemistry of granitoids associated with the northern ophiolite mélange of central Cuba: Tectonic implication for late Cretaceous magmatism in the northwestern Caribbean. Am. J. Sci. 310, 1453–1479. https://doi.org/10.2475/10.2010.09.

Rojas-Agramonte, Y., Kröner, A., Garcia-Casco, A., Somin, M., Iturralde-Vinent, M., Mattinson, J.M.M., Millán Trujillo, G., Sukar, K., Pérez Rodríguez, M., Carrasquilla, S., Wingate, M.T.D.T.D., Liu, D.Y.Y., 2011. Timing and evolution of cretaceous island arc magmatism in central Cuba: implications for the history of arc systems in the northwestern Caribbean. J. Geol. 119, 619–640. https://doi.org/10.1086/662033.

Rojas-Agramonte, Y., Garcia-Casco, A., Kemp, A., Kröner, A., Proenza, J.A., Lázaro, C., Liu, D., 2016. Recycling and transport of continental material through the mantle wedge above subduction zones: a Caribbean example. Earth Planet. Sci. Lett. 436, 93–107. https://doi.org/10.1016/J.EPSL.2015.11.040.

Rui, H.C., Yang, J.S., Zheng, J.P., Llanes Castro, A.I., Liu, F., Wu, Y., Wu, W.W., Valdes Mariño, Y., Masoud, A.E., 2022. Early Cretaceous subduction initiation of the proto-Caribbean plate: geochronological and geochemical evidence from gabbros of the Moa-Baracoa ophiolitic massif, Eastern Cuba. Lithos 418–419, 106674. https://doi.org/10.1016/j.lithos.2022.106674.

Saha, A., Basu, A.R., Wakabayashi, J., Wortman, G.L., 2005. Geochemical evidence for a subducted infant arc in Franciscan high-grade-metamorphic tectonic blocks. Bull. Geol. Soc. Am. 117, 1318–1335. https://doi.org/10.1130/B25593.1.

Salters, V.J.M., Stracke, A., 2004. Composition of the depleted mantle. Geochemistry, Geophys. Geosystems 5, Q05B07. https://doi.org/10.1029/2003GC000597.

Saura, E., Vergés, J., Brown, D., Lukito, P., Soriano, S., Torrescusa, S., García, R., Sánchez, J.R., Sosa, C., Tenreyro, R., 2008. Structural and tectonic evolution of western Cuba fold and thrust belt. Tectonics 27, TC4002. https://doi.org/10.1029/2007TC002237.

Savov, I.P., Ryan, J.G., D'Antonio, M., Kelley, K., Mattie, P., 2005. Geochemistry of serpentinized peridotites from the Mariana Forearc Conical Seamount, ODP Leg 125: implications for the elemental recycling at subduction zones. Geochemistry, Geophys. Geosystems 6, Q04J15. https://doi.org/10.1029/2004GC000777.

Scambelluri, M., Tonarini, S., 2012. Boron isotope evidence for shallow fluid transfer across subduction zones by serpentinized mantle. Geology 40, 907–910. https://doi.org/10.1130/G33233.1.

Scambelluri, M., Rampone, E., Piccardo, G.B., 2001. Fluid and element cycling in subducted serpentinite: a trace-element study of the Erro-Tobbio high-pressure ultramafites (Western Alps, NW Italy). J. Petrol. 42, 55–67. https://doi.org/10.1093/petrology/42.1.55.

Scambelluri, M., Fiebig, J., Malaspina, N., Müntener, O., Pettke, T., 2004. Serpentinite subduction: implications for fluid processes and trace-element recycling. Int. Geol. Rev. 46, 595–613. https://doi.org/10.2747/0020-6814.46.7.595.

Scambelluri, M., Cannaò, E., Gilio, M., 2019. The water and fluid-mobile element cycles during serpentinite subduction. A review. Eur. J. Mineral. 31, 405–428. https://doi.org/10.1127/EJM/2019/0031-2842.

Schmidt, M.W., Poli, S., 2014. Devolatilization during subduction. In: Treatise on Geochemistry: Second Edition, pp. 669–701. https://doi.org/10.1016/B978-0-08-095975-7.00321-1.

Schneider, J., 2000. Origines et chemins P, T, t d'éclogites de Cuba (Villa Clara) exhumes en contexte de subduction. Montpellier II.

Schneider, J., Bosch, D., Monié, P., Guillot, S., Garcia-Casco, A., Lardeaux, J.M., Torres-Roldán, R.L., Trujillo, G.M., 2004. Origin and evolution of the Escambray Massif (Cenral Cuba): an example of HP/LT rocks exhumed during intraoceanic subduction. J. Metamorph. Geol. 22, 227–247. https://doi.org/10.1111/j.1525-1314.2004.00510.x.

Scott, J.M., Smith, S.A., Tarling, M.S., le Roux, P.J., Harris, C., Hoffmann, J.E., Scherzer, S., Tulley, C.J., 2019. Element and Sr–O isotope redistribution across a plate boundary-scale crustal serpentinite mélange shear zone, and implications for the slab-mantle interface. Earth Planet. Sci. Lett. 522, 198–209. https://doi.org/10.1016/j.epsl.2019.06.034.

Snow, J.E., Hart, S.R., Dick, H.J.B., 1994. Nd and Sr isotope evidence linking mid-ocean-ridge basalts and abyssal peridotites. Nature 371, 57–60. https://doi.org/10.1038/371057a0.

Somin, M., Millán, G., 1981. Geology of the Metamorphic Complexes of Cuba. Nauka Press, USSR, Moscow.

Sorensen, S.S., 1988. Petrology of amphibolite-facies mafic and ultramafic rocks from the Catalina Schist, southern California: metasomatism and migmatization in a subduction zone metamorphic setting. J. Metamorph. Geol. 6, 405–435. https://doi.org/10.1111/j.1525-1314.1988.tb00431.x.

Sorensen, S.S., Grossman, J.N., 1989. Enrichment of trace elements in garnet amphibolites from a paleo-subduction zone: Catalina Schist, southern California. Geochim. Cosmochim. Acta 53, 3155–3177. https://doi.org/10.1016/0016-7037(89)90096-3.

Sorensen, S.S., Grossman, J.N., Perfit, M.R., 1997. Phengite-hosted LILE enrichment in eclogite and related rocks: Implications for fluid-mediated mass transfer in subduction zones and arc magma genesis. J. Petrol. 38, 3–34. https://doi.org/10.1093/petroj/38.1.3.

Sorensen, S.S., Sisson, V.B., Harlow, G.E., Avé Lallemant, H.G., 2010. Element residence and transport during subduction-zone metasomatism: evidence from a jadeitite-serpentinite contact, Guatemala. Int. Geol. Rev. 52, 899–940. https://doi.org/10.1080/00206810903211963.

Soret, M., Agard, P., Dubacq, B., Vitale-Brovarone, A., Monié, P., Chauvet, A., Whitechurch, H., Villemant, B., 2016. Strain localization and fluid infiltration in the mantle wedge during subduction initiation: evidence from the base of the New Caledonia ophiolite. Lithos 244, 1–19. https://doi.org/10.1016/j.lithos.2015.11.022.

Spandler, C., Pirard, C., 2013. Element recycling from subducting slabs to arc crust: a review. Lithos 170–171, 208–223. https://doi.org/10.1016/j.lithos.2013.02.016.

Spandler, C., Pettke, T., Rubatto, D., 2011. Internal and external fluid sources for eclogite-facies veins in the Monviso Meta-ophiolite, Western Alps: implications for fluid flow in subduction zones. J. Petrol. 52, 1207–1236. https://doi.org/10.1093/petrology/egr025.

Stanek, K.P., Maresh, W.V., Grafe, F., Grevel, C., Baumann, A., 2006. Structure, tectonics and metamorphic development of the Sancti Spiritus Dome (eastern Escambray massif, Central Cuba). Geol. Acta 4, 151–170.

Stanek, K.P., Maresch, W.V., Scherer, E., Krebs, M., Berndt, J., Sergeev, S.S., Rodionov, N., Pfänder, J., Hames, W.E., 2019. Born in the Pacific and raised in the Caribbean: construction of the Escambray nappe stack, central Cuba. A review. Eur. J. Mineral. 31, 5–34. https://doi.org/10.1127/ejm/2019/0031-2795.

Taetz, S., John, T., Bröcker, M., Spandler, C., 2016. Fluid–rock interaction and evolution of a high-pressure/low-temperature vein system in eclogite from New Caledonia: insights into intraslab fluid flow processes. Contrib. to Mineral. Petrol. 171, 1–27. https://doi.org/10.1007/s00410-016-1295-z.

Tarling, M.S., Smith, S.A., Scott, J.M., 2019. Fluid overpressure from chemical reactions in serpentinite within the source region of deep episodic tremor. Nat. Geosci. 12, 1034–1042. https://doi.org/10.1038/s41561-019-0470-z.

Thompson, J.B., 1982. Composition space: an algebraic and geometric approach. In: Ferry, J.M. (Ed.), Characterization of Metamorphism through Mineral Equilibria. Mineralogical Society of America, Reviews in Mineralogy, 10, pp. 1–31.

Torres-Roldan, R.L., Garcia-Casco, A., Garcia-Sanchez, P.A., 2000. CSpace: an integrated workplace for the graphical and algebraic analysis of phase assemblages on 32-bit wintel platforms. Comput. Geosci. 26, 779–793. https://doi.org/10.1016/S0098-3004(00)00006-6.

Ukar, E., Cloos, M., 2013. Actinolitic rinds on low-T mafic blueschist blocks in the Franciscan shale-matrix mélange near San Simeon: Implications for metasomatism and tectonic history. Earth Planet. Sci. Lett. 377–378, 155–168. https://doi.org/10.1016/j.epsl.2013.06.038.

van der Straaten, F., Schenk, V., John, T., Gao, J., 2008. Blueschist-facies rehydration of eclogites (Tian Shan, NW-China): implications for fluid-rock interaction in the subduction channel. Chem. Geol. 255, 195–219. https://doi.org/10.1016/j.chemgeo.2008.06.037.

van Hinsbergen, D.J.J., Iturralde-Vinent, M.A., van Geffen, P.W.G., Garcia-Casco, A., van Benthem, S., 2009. Structure of the accretionary prism, and the evolution of the Paleogene northern Caribbean subduction zone in the region of Camagüey, Cuba. J. Struct. Geol. 31, 1130–1144. https://doi.org/10.1016/j.jsg.2009.06.007.

Van Keken, P.E., Hacker, B.R., Syracuse, E.M., Abers, G.A., 2011. Subduction factory: 4. Depth-dependent flux of H2O from subducting slabs worldwide. J. Geophys. Res. Solid Earth 116, B01401. https://doi.org/10.1029/2010JB007922.

Veizer, J., Ala, D., Azmy, K., Bruckschen, P., Buhl, D., Bruhn, F., Garden, G.A.F., Diener, A., Ebneth, S., Godderis, Y., Jasper, T., Korte, C., Pawellek, F., Podlaha, O.G., Strauss, H., 1999. 87Sr/86Sr, δ13C and δ18O evolution of Phanerozoic seawater. Chem. Geol. 161, 59–88. https://doi.org/10.1016/S0009-2541(99)00081-9.

Vitale-Brovarone, A., Alard, O., Beyssac, O., Martin, L., Picatto, M., 2014. Lawsonite metasomatism and trace element recycling in subduction zones. J. Metamorph. Geol. 32, 489–514. https://doi.org/10.1111/jmg.12074.

Whitney, D.L., Evans, B.W., 2010. Abbreviations for names of rock-forming minerals. Am. Mineral. 95, 185–187. https://doi.org/10.2138/am.2010.3371.

Zack, T., John, T., 2007. An evaluation of reactive fluid flow and trace element mobility in subducting slabs. Chem. Geol. 237, 5–22. https://doi.org/10.1016/j.chemgeo.2006.06.013.